Journal of Human Evolution 133 (2019) 78–98

Contents lists available at ScienceDirect

Journal of Human Evolution

journal homepage: www.elsevier.com/locate/jhevol

A multiscale stratigraphic investigation of the context of StW 573 'Little Foot' and Member 2, Sterkfontein Caves, South Africa

Laurent Bruxelles [a, b, c, *], Dominic J. Stratford [c], Richard Maire [d], Travis R. Pickering [e, f], Jason L. Heaton [f, g], Amelie Beaudet [c, h], Kathleen Kuman [c], Robin Crompton [f, i, j], Kris J. Carlson [f, k], Tea Jashashvili [f, l, m], Juliet McClymont [n], George M. Leader [c, o, p], Ronald J. Clarke [f]

[a] INRAP, French Institute for Preventive Archaeological Researches, 561 rue Etienne Lenoir, km delta, 30900, Nîmes, France
[b] IFAS, French Institute of South African Studies, 62 Juta Street, Braamfontein, Johannesburg, South Africa
[c] School of Geography, Archaeology and Environmental Studies, University of Witwatersrand, WITS 2050, Johannesburg, Gauteng, South Africa
[d] UMR 5319 Passages, CNRS-University of Bordeaux and Bordeaux-Montaigne, France
[e] Department of Anthropology, University of Wisconsin, Madison, WI, 53706, USA
[f] Evolutionary Studies Institute, University of Witwatersrand, WITS 2050, Johannesburg, Gauteng, South Africa
[g] Department of Biology, Birmingham-Southern College, Birmingham, AL, 35254, USA
[h] Department of Anatomy, University of Pretoria, PO Box 2034, Pretoria, 0001, South Africa
[i] Department of Musculoskeletal Biology, Institute of Ageing and Chronic Disease, University of Liverpool, The William Henry Duncan Building, 6 West Derby Street, Liverpool, L7 8TX, UK
[j] Department of Rheumatology, Aintree University Hospital NHS Trust, Liverpool, L9 7AL, UK
[k] Department of Integrative Anatomical Sciences, Keck School of Medicine, University of Southern California, Los Angeles, CA, 90033, USA
[l] Molecular Imaging Center, Department of Radiology, Keck School of Medicine, University of Southern California, Los Angeles, CA, 90033, USA
[m] Department of Geology and Paleontology, Georgian National Museum, Tbilisi, 0105, Georgia
[n] Centre for Health Research, School of Health Sciences, University of Brighton, UK
[o] Department of Sociology and Anthropology, The College of New Jersey, Ewing, NJ, USA
[p] Department of Anthropology, University of Pennsylvania, Philadelphia, PA, USA

ARTICLE INFO

Article history:
Received 7 August 2018
Accepted 16 May 2019

Keywords:
StW 573
Australopithecus
Sterkfontein
Member 2
Stratigraphy
Cave geology

ABSTRACT

The Sterkfontein Caves is currently the world's richest *Australopithecus*-bearing site. Included in Sterkfontein's hominin assemblage is StW 573 ('Little Foot'), a near-complete *Australopithecus* skeleton discovered in Member 2 in the Silberberg Grotto. Because of its importance to the fossil hominin record, the geological age of StW 573 has been the subject of significant debate. Three main hypotheses have been proposed regarding the formation and age of Member 2 and by association StW 573. The first proposes that Member 2 (as originally defined in the type section in the Silberberg Grotto) started to accumulate at around 2.58 Ma and that the unit is contained within the Silberberg Grotto. The second proposes that Member 2 started forming before 3.67 ± 0.16 Ma and that the deposit extends into the Milner Hall and close to the base of the cave system. The third proposes a 'two-stage burial scenario', in which some sediments and StW 573 represent a secondary and mixed-age accumulation reworked from a higher cave. The stratigraphic and sedimentological implications of these hypotheses are tested here through the application of a multiscale investigation of Member 2, with reference to the taphonomy of the StW 573 skeleton. The complete infilling sequence of Member 2 is described across all exposures of the deposit in the Silberberg Grotto and into the Milner Hall. Sediments are generally stratified and conformably deposited in a sequence of silty sands eroded from well-developed lateritic soils on the landscape surface. Voids, clasts and bioclasts are organized consistently across and through Member 2 conforming with the underlying deposit geometry, indicating gradual deposit accretion with no distinct collapse facies evident and only localized intra-unit postdepositional modification. The stratigraphy and sedimentology of Member 2 support a simple single-stage accumulation process of Member 2 and a primary association between the sediments of Member 2 and the StW 573 'Little Foot' skeleton.

© 2019 Elsevier Ltd. All rights reserved.

* Corresponding author.
E-mail address: laurent.bruxelles@inrap.fr (L. Bruxelles).

https://doi.org/10.1016/j.jhevol.2019.05.008
0047-2484/© 2019 Elsevier Ltd. All rights reserved.

1. Introduction

The Sterkfontein Caves, located about 50 km north-west of Johannesburg, South Africa are situated on the southern side of the Bloubank River in the south-western area of the Cradle of Humankind World Heritage Site. Over the last 80 years, the caves of the Cradle of Humankind (COH) have yielded some of the most significant hominin discoveries representing three genera and potentially five species spanning possibly 4 Ma (maximum age based on Partridge et al., 2003; see below for discussion). The sedimentary sequence used by researchers to divide the Sterkfontein deposits into chronostratigraphic units was developed by Partridge (1978, 2000) and is referred to as the 'Sterkfontein Formation' (see also Stratford, 2017 for a review). This sequence comprises six members ordered stratigraphically (although in no single exposure are all members represented), with Member 1 at the base and Member 6 at the top. Members 2 through 6 represent allogenic fillings. Member 1 consists of an autogenic filling developed internally through cave breakdown before a significant opening to the surface had formed. The majority of hominin specimens found at Sterkfontein is attributed to the genus *Australopithecus* and have been yielded from the Member 4 deposits of the Sterkfontein Formation (Partridge, 1978). Deeper chambers have yielded *Australopithecus* specimens of potentially Pliocene age (Clarke, 1998, 2013; Partridge et al., 2003; Beaudet et al., 2018); see below for discussion on the geological age of the specimens). The most complete of the Sterkfontein hominin specimens is StW 573 ('Little Foot'), a partial *Australopithecus* skeleton excavated from the Member 2 deposit (Clarke, 1998) found in the Silberberg Grotto (Fig. 1).

Sterkfontein Member 2 has been the subject of intense debate since the discovery of the StW 573 (Clarke, 1998). Debate has centered largely around the age of the specimen (Clarke and Tobias, 1995; McKee, 1996; Tobias and Clarke, 1996; Turner, 1997; Partridge et al., 1999, 2003; Berger et al., 2002; Clarke, 2002a,b; Clarke et al., 2003; Partridge, 2005; Walker et al., 2006; Pickering and Kramers, 2010; Pickering et al., 2010, 2011; Herries and Shaw, 2011; Granger et al., 2015; Kramers and Dirks, 2017a,b; Stratford et al., 2017), and it has necessarily included discussion of the stratigraphic history of StW 573 and Member 2 (Clarke, 1998, 2002a,b, 2006, 2007, 2008; Pickering and Kramers, 2010; Bruxelles et al., 2014; Kramers and Dirks, 2017a,b; Stratford et al., 2017). Member 2 is the basal allogenic unit of the Sterkfontein Formation. It was originally described by Partridge (1978) from exposures in the Silberberg Grotto, one of the deeper chambers in the Sterkfontein cave system which overlies 5 km of passages and chambers (including the Milner Hall and Elephant Chamber; Martini et al., 2003). Although debate continues about the geological age of Member 2, some data suggest it may represent the oldest *Australopithecus*-bearing deposit of the Sterkfontein Formation (e.g., Clarke, 2002a; Partridge et al., 2003; Granger et al., 2015). The geological age of Member 2 and StW 573 has significant implications for not only where StW 573 lies in hominin phylogeny, but also for the maximum age of deposits at Sterkfontein and the process of formation of the caves themselves. Various hypotheses have been proposed regarding the geological age of StW 573 and its stratigraphic history in relation to the evolution of the caves. These are summarized here and discussed in detail below. U-Pb and palaeomagnetic studies suggest: that Member 2 (from samples within the Silberberg Grotto as opposed to borehole samples used by Pickering and Kramers, 2010) accumulated from about 2.58 Ma (Walker et al., 2006; Herries and Shaw, 2011; Herries et al., 2013) and is contemporaneous with Member 4; that some of the sediments in the western Silberberg Grotto may not be Member 2 (Pickering and Kramers, 2010); that Member 2 may extend laterally beyond the Silberberg Grotto (in boreholes 4, 1, 5 and 3?; Pickering and Kramers, 2010); and that Member 2 does not extend deeper than the Silberberg Grotto. This final hypothesis supports proposals for an epiphreatic[1] karstification process forming the caves (Partridge, 1978; Partridge and Watt, 1991; Pickering and Kramers, 2010; Herries et al., 2013), i.e., deeper networks are formed later and necessarily filled with younger or reworked sediments. It must be noted that the deposits identified in the boreholes are not stratigraphically calibrated to the type section of Member 2 as described by Partridge (1978) and so may or may not belong to Member 2.

Granger et al. (2015) applied cosmogenic nuclide isochron dating to 11 samples comprising clasts and sediments stratigraphically associated with StW 573. The results revealed a geological age of 3.67 ± 0.16 Ma for the sediments containing StW 573. From the cosmogenic samples, Granger et al. (2015) proposed a slow landscape erosion rate. Kramers and Dirks (2017a, b) suggested that one of the 11 samples included in the isochron published by Granger et al. (2015) could indicate reworking of some sediments in Member 2. They argued that a two-stage burial scenario involving a collapse of sediments from an upper chamber containing the StW 573 skeleton would explain this anomalous sample (see Stratford et al., 2017 for reply).

Sedimentological evidence from exposures of Member 2 in the Silberberg Grotto should preserve evidence of the mode of accumulation and extent of the deposit. These exposures, therefore, can be used to test the hypotheses presented by Pickering and Kramers (2010) and Kramers and Dirks (2017a, b), elucidate the associated taphonomic implications for the StW 573 skeleton, and associate sedimentological features with depositional processes and surface geomorphological contexts. Refining the stratigraphic history of Member 2 improves our understanding of the formation and opening of the caves and the local geomorphological, ecological and environmental conditions during its infilling, thereby providing a more nuanced contextual framework for hominin evolution in southern Africa during the Plio-Pleistocene. Research presented here draws on multiscale and multidisciplinary evidence to further clarify the stratigraphic context of Member 2 and the association of StW 573 within that unit.

1.1. Previous interpretations of Member 2 stratigraphy

Partridge (1978) first described Member 2 from exposures in the Silberberg Grotto (Fig. 1a, b). The morphology of the Silberberg Grotto is defined by the strong east to west fault-guided cavity development that characterizes the Sterkfontein system (Martini et al., 2003; Stratford, 2017; Bruxelles, 2018). The chamber has developed along the southern boundary of the cave system and extends approximately 30 m east to west. To the west, the chamber divides into three smaller passages that continue west and open into the underlying Elephant Chamber and Milner Hall (Fig. 1b). The northern and eastern extents of the chamber are unknown as these walls are comprised of breccia,[2] remnants of mined speleothem,

[1] An epiphreatic karstification model involves the dissolution of soluble host rock and mechanical removal of sediments in the uppermost phreatic zone (the water table level including its fluctuations) where circulation of water is greatest, as is the rate of karstification. In a traditional epiphreatic kartification model, lowering of the water table associated with denudation of the landscape causes the caves to deepen and form successively lower passages and chambers—the lower passages and chambers being the youngest in the system.

[2] The term 'breccia' here describes sedimentary breccia deposits which consist of angular to subangular, poorly sorted clasts (>2 mm) contained within a matrix (<2 mm) of smaller particles and cementing minerals. When most of the clasts are <2 mm we use the term microbreccia to describe matrix-supported cemented sediments composed mostly of sand-sized mineral angular particles.

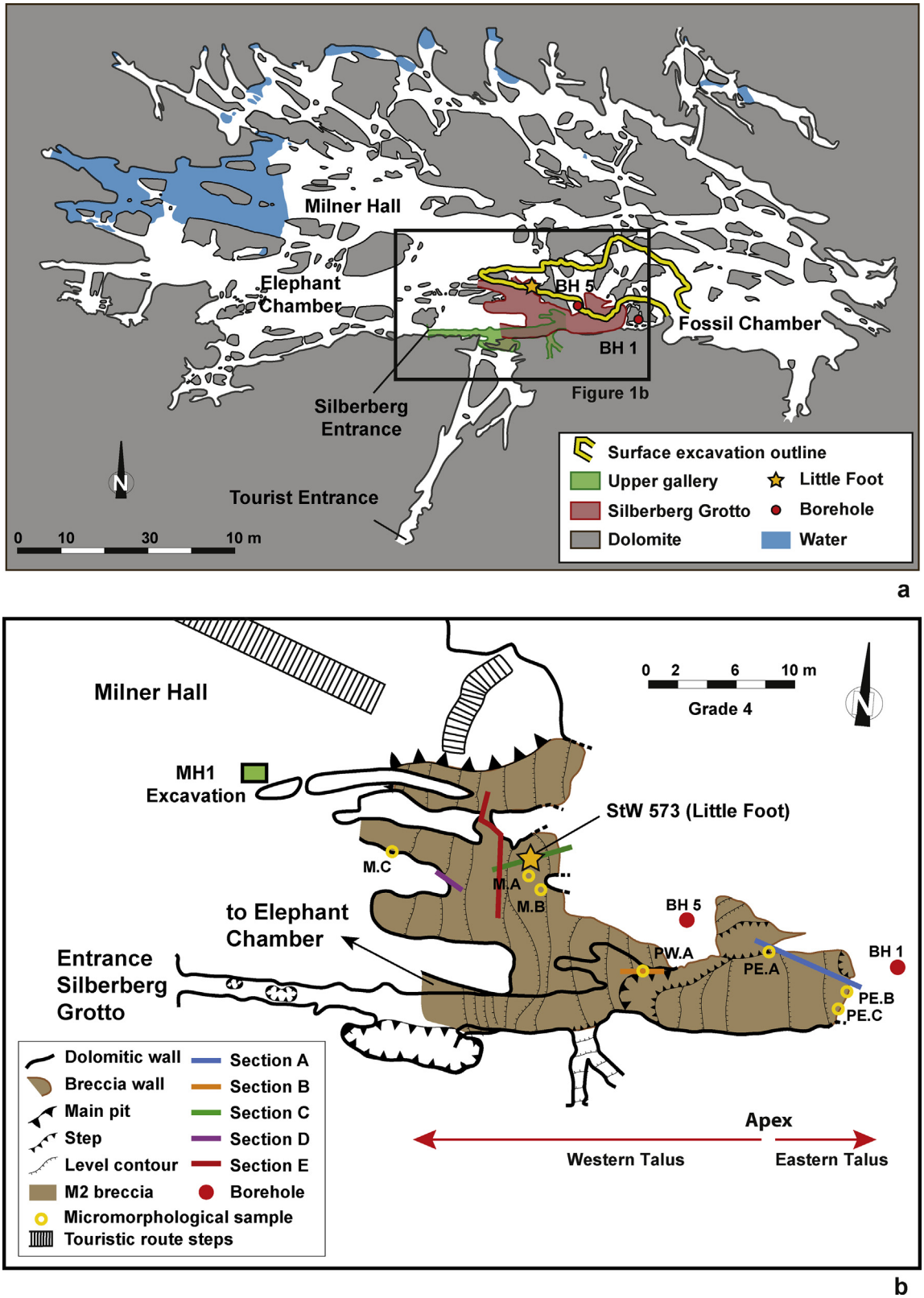

Figure 1. a) General plan of Sterkfontein caves (from Martini et al., 2003). b) Plan of the Silberberg Grotto with openings to associated chambers, talus topography, locations of described sections and sediment micromorphology samples. Star indicates location of StW 573. Adjusted from Bruxelles et al. (2014).

and dolomite pendants. Based on the proximity of the Name Chamber to the north (Martini et al., 2003), it is likely the chamber's northern extent is limited to less than 20 m from the southern wall. The large talus cone of Member 2 was deposited on the thick flowstone covering the irregular surface of the autogenic Member 1 (Partridge, 1978, 2000; Martini et al., 2003). Several researchers have described the morphology of Member 2 in relation to its formation and proposed that the deposit accumulated from an aven-like opening high in the roof above the eastern area of the chamber (Partridge, 1978; Martini et al., 2003; Clarke, 2006). The east and west flanks of Member 2 slope away from this point (Fig. 1a). StW 573 was discovered about 18 m down the steeper western slope (Fig. 1a; Clarke, 2006; Bruxelles et al., 2014).

In his seminal stratigraphic work, Partridge (1978) placed Member 2 at the base of the fossiliferous sequence. Underlying Member 2 is Member 1 and a variably associated speleothem. This unit has been most notably described, albeit briefly, by Partridge (1978, 2000), Partridge and Watt (1991), Martini et al (2003), Clarke (2006), and Pickering and Kramers (2010). The clastic component of Member 1 is consistently described as a collapse breccia dominated by unorganized, angular dolomitic and chert blocks in a manganiferous matrix containing stalagmitic and lenticular speleothems. The unit formed through the vadose breakdown of the cave prior to significant opening to the surface. Partridge (1978) originally recognized a contamination of allogenic clastic material and bone in the upper reaches (described similarly in Pickering and Kramers, 2010), but this was not noted by Martini (2003) or Clarke (2006). The contact between Member 1 and the overlying Member 2 is variable. In boreholes 1 and 4, Pickering and Kramers (2010) proposed a speleothem unit separating Member 1 from 2 (they did not identify a speleothem present at this contact in boreholes 3 and 5). From exposures in the Silberberg Grotto, Partridge (1978) did not describe a speleothem present at the contact, although he did describe "a large stalagmitic boss belonging to Member 1" (Partridge, 1978: 284), and Clarke (2006: 115) described Member 1 as "a collapsed debris pile of large roof blocks cemented with flowstone". Clarke (2006) proposed the general formation of a speleothem 'boss' on Member 1, on which Member 2 formed. Where this speleothem is present and interstratifying Members 1 and 2, we associate this speleothem with a stage of Member 1 formation during a period prior to significant opening of the caves to the surface. Hence this is a pre-Member 2 unit. We refer to this speleothem as a 'boss' speleothem.

From exposures in the eastern Silberberg Grotto and the "east pit of the type site", Partridge (1978: 284) identified a thick allogenic unit overlying Member 2, which he named Member 3. A flowstone named Unit '3A' separated the two members and was exposed in the roof of the Silberberg Grotto (Partridge, 1978; Partridge and Watt, 1991). Martini et al. (2003) described this unit as a relatively regular and widespread flowstone sheet. Member 3 is not visible in the western Silberberg Grotto, and the interbedding flowstone named by Partridge as Unit 3A is also absent in the western area. Pickering and Kramers (2010) abandoned Member 3 as a valid member and so did not recognize the same flowstones as Partridge (1978) and Partridge and Watt (1991) as upper Member 2, Member 3 or lower Member 4 sequence boundaries. A thicker flowstone is identified from cores as separating Members 2 and 4 (sample BH4-9 in Pickering and Kramers, 2010). We do recognize, in the Silberberg Grotto, the deposit-separating speleothem identified as Unit 3A by Partridge (1978) and Martini et al. (2003). Because the boundaries recognized in cores used by Partridge and Watt (1991) and Pickering and Kramers (2010) cannot be calibrated to the type section exposure in the eastern Silberberg Grotto (Partridge, 1978), we follow the original section used by Partridge (1978) as representing the upper limit of Member 2 in the Silberberg Grotto. Although Member 3 is not the subject of this research, in the stratigraphic sections presented here we document the contact between Member 2 and Member 3 where visible. While Pickering and Kramers (2010) have questioned if Member 3 is distinct from the overlying Member 4, we do not attempt to address this question as our focus is on Member 2.

Member 2 was described as a well-bedded, silty-loam matrix-supported talus of up to 5 m depth, with 'sparse rock debris' and localized abundant bone. The western slope was interpreted by Partridge (1978: 284) as accumulating through a "conical gravitative accretion." On the eastern side of the talus apex (Fig. 1), the bone-rich, shallower dipping eastern flank was deposited under fluid-driven sedimentation (Partridge, 1978; Partridge and Watt, 1991). Partridge (1978, 2000) clearly identified the upper limit of Member 2 in the eastern Silberberg Grotto as sealed by a flowstone that represents the first unit of Member 3 ('Bed A' of Member 3 in Partridge, 1978; 'SA-7' in our sections). The clastic sediments of Member 2 and Member 3 are distinctly separated in the Silberberg Grotto, and we consider them different deposits. Below we summarize work referring to Member 2 and do not consider Member 3 as playing a role in the mode of deposition or morphology of the stratigraphically lower Member 2.

Following the discovery of StW 573, Clarke (2002b, 2006: 115) described the specimen as "embedded in a very stony breccia" interbedded with thin calcite layers and dark brown calcified mudstone, proposing a detailed formation scenario for Member 2 and the sediments directly associated with StW 573. Martini et al. (2003) estimated the maximum thickness of Member 2 as 8 m and described the deposit similarly to Partridge (1978) and Partridge and Watt (1991) but placed greater emphasis on deposition of sediment by "stream action" (Martini et al., 2003: 58). Pickering and Kramers (2010) also proposed a possible maximum thickness for Member 2 of 8 m (in Borehole 1) and described the deposit as a "pocket of coarse-grained, blocky, dolomite-rich rock debris in a reddish-brown sandy matrix with several inter-bedded flowstone layers" (Pickering and Kramers, 2010: 81, Table 6). However, they also noted that Borehole 1 does not transect the Silberberg Grotto and so may not reach or sample what was considered to be Member 2 in the original description.

Pickering and Kramers (2010) attributed the sediments around StW 573 to 'Facies A'—interpreted as a proximal talus facies near the StW 573 specimen. More eastern sediments were attributed to 'Facies C'—interpreted as distal talus facies. This suggests that the sediments containing StW 573 were associated with a local 'pocket' of proximal Member 2 sediments closely associated with distal sediments of another deposit ('Member 2?'; see Pickering and Kramers, 2010: Fig. 3).

In contrast, Bruxelles et al. (2014) examined the sediments of Member 2 associated with the StW 573 skeleton and identified a stratified sequence of three clastic units (B1, B2a,b and B3) and five speleothemic units (F1, F2, F3, F4a,b and F5). Clasts increase in abundance in B2b and B3, but the matrix is generally identified as 'clayey sand'. Localized cavities have formed in all clastic units and were subsequently filled with speleothem, a process observed by Clarke (2002b) and documented in detail by Bruxelles et al. (2014). Such cavities are associated with episodic increases in fresh water throughput, localized pooling of water, and flushing of poorly indurated sediments (Partridge, 1978; Clarke, 2002b, 2006; Martini et al., 2003; Bruxelles et al., 2014). These processes caused the localized vertical displacement of the central part of the StW 573 skeleton.

Regarding the possible extension of Member 2 beyond the Silberberg Grotto, Partridge (1978) and Partridge and Watt (1991) considered the underlying passages and chambers, like the Elephant Chamber and Milner Hall to have formed after the

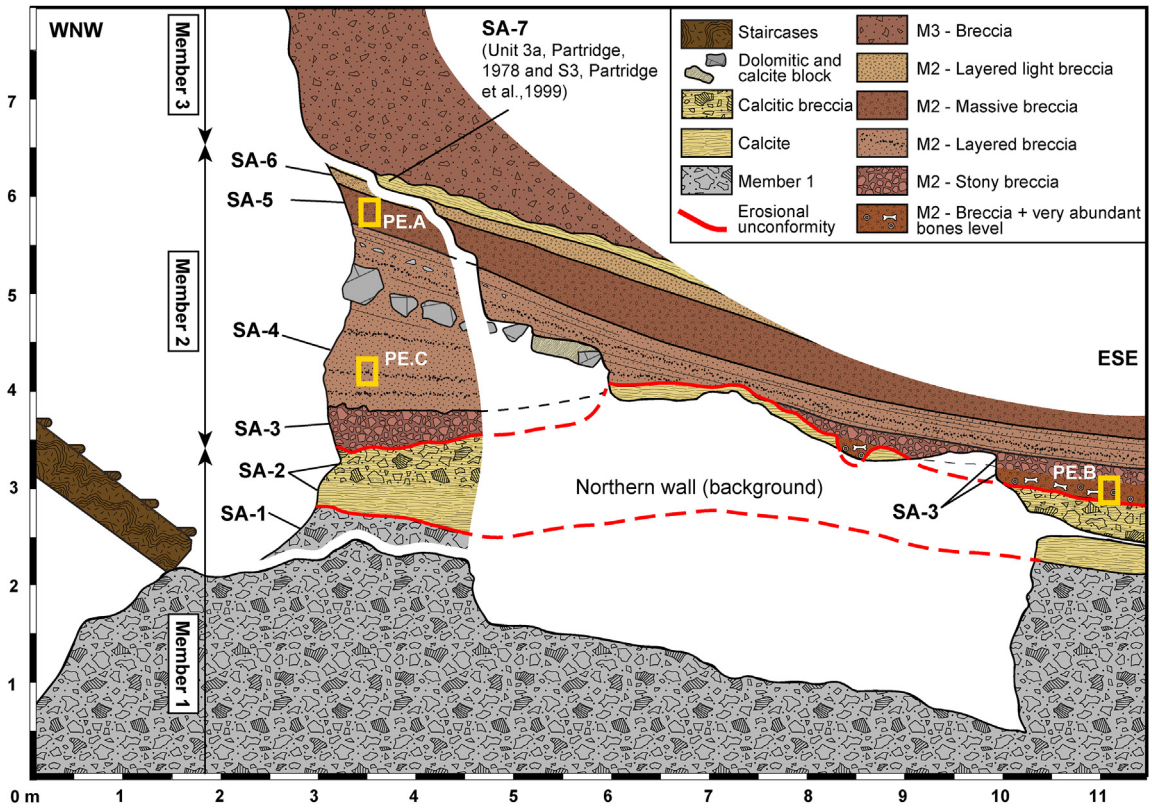

Figure 2. Synthetic representation of Section A (see Fig. 1b for location).

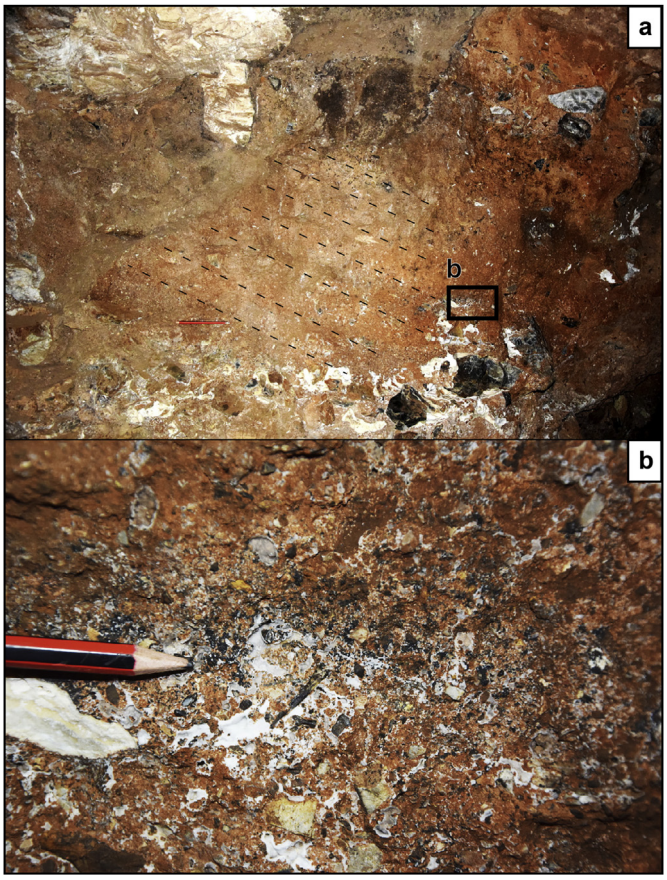

Figure 3. a) Section A of the Eastern talus. b) Stratified deposits with microfauna rich layers.

Silberberg Grotto through speleogenesis resulting from a lowering of the base level associated with an epiphreatic karstification model. They considered that all deposits contained in the chambers and passages underlying the Silberberg Grotto must be either formed from reworked old sediments, or formed by younger sediments deposited to the base of the system through the numerous aven-style openings that currently feed sediments from the surface to the lower levels of the cave system. This hypothesis has more recently been supported by U-Th dates of seven samples of flowstones covering talus deposits found near the base of the cave system in the Milner Hall and Jacovec Cavern and dating to younger than 400 ka (Pickering and Kramers, 2010).

Wilkinson's geomorphological work (1973, 1983, 1985) argued that the Jacovec Cavern sediments and Silberberg Grotto deposits extend close to the current base level. He thus proposed that the deepest deposits, which are found in the Jacovec Cavern and Milner Hall (as a proposed extension of the Member 2 deposit exiting the Silberberg Grotto), are some of the oldest. This model has been supported by recent stratigraphic work conducted in the Milner Hall (Stratford et al., 2014) and by preliminary cosmogenic nuclide dates of 3.76 ± 0.26–4.02 ± 0.27 Ma for hominin-bearing deposits in the Jacovec Cavern (Partridge et al., 2003).

1.2. Member 2 age and implications for deposit formation

Significant attention has centered on the dating of the StW 573 skeleton. Application of a range of methods including biochronology (e.g., Clarke and Tobias, 1995; McKee, 1996; Turner, 1997; Clarke, 1998, 2002a; Berger et al., 2002), U-series dating (e.g., Walker et al., 2006; Pickering and Kramers, 2010), paleomagnetic dating (e.g., Partridge et al., 1999, 2000; Herries and Shaw, 2011) and cosmogenic nuclide dating (Partridge et al.,

2003; Granger et al., 2015) produced dates from a maximum of 4.02 ± 0.27 Ma (Partridge et al., 2003) to a minimum of 1.07–1.95 Ma (McKee, 1996; Berger et al., 2002; see Tobias and Clarke, 1996 and Clarke, 2002a for respective replies).

Inside the Silberberg Grotto, flowstone samples produced U-Pb dates of 2.31–2.17 Ma for the speleothem below the specimen (speleothem '2B' in Walker et al., 2006). For the same flowstone, Pickering and Kramers (2010) yielded an age of 2.35 ± 0.10 Ma. The flowstone directly associated with StW 573 (speleothem '2C' in Walker et al., 2006) yielded dates of 2.33–2.06 Ma and is generally cited as 2.2 Ma (Walker et al., 2006). Paleomagnetic dates have three options depending on the calibration of the sequence (Partridge et al., 2000; Herries et al., 2013). Option 'A' (Herries et al., 2013) calibrates the top of the sequence (sample 'S3') at 2.58 to 3.03–3.12 Ma for sample '2D', with the basal speleothem covering Member 1 (sample 'S1') dating to 3.11 Ma and fitting within the Kaena reversed to Gauss normal polarity event. Speleothem '2C' (intruding through the unit and StW 573) formed during the Reunion, Huckleberry Ridge normal short polarity event and dates to 2.16–2.05 Ma. Option 'B' (Herries et al., 2013) calibrates the paleomagnetic sequence at the top to the Olduvai normal polarity event dated to 1.78–1.95 Ma for speleothem sample 'S3' and '2D' respectively, and at the base to the Matayama reversed polarity event (Member 1 speleothem sample 'S1'), dated to 2.58 Ma. The intrusive flowstone '2C' is interpreted as forming within the Reunion, Huckleberry Ridge normal polarity event. Option 'B' has been proposed to be the more likely of the options based on the coherence of the U-Pb dates to speleothem samples '2B' and '2C' (see Herries et al., 2013). Option 'C' (Partridge et al., 2000) places flowstone '2B', just below the specimen, at the Gauss (normal polarity) Gilbert (reversed polarity) event at 3.60 Ma (Ogg, 2012). Although authors acknowledge that the '2C' flowstone dated to 2.2 Ma formed after the deposition of the skeleton (Partridge et al., 2000; Walker et al., 2006; Pickering and Kramers, 2010; Herries and Shaw, 2011; Herries et al., 2013), Partridge et al. (2000:129) proposed that the other flowstones in the vicinity (2A, 2B, 2D and 3) were "locally continuous" and "interbedded conformably". Stratigraphic considerations of these flowstones presented by Clarke (2002b) and Bruxelles et al. (2014) demonstrated that speleothems '2B', '2C' and '2D' are postdepositional void-infilling flowstones that cannot directly date the skeleton or associated sediments but only provide a minimum age for the deposits. They do, however, provide some interesting insights in the void-forming erosional phases in the Silberberg Grotto that can potentially be linked to other similarly-aged flowstones elsewhere in the sequence that formed in the same generation of void-filling post-sequence-wide erosion and subsidence.

Outside the Silberberg Grotto, Pickering and Kramers (2010) used flowstones present in boreholes to define the Member 2 sequence based on packages with similar lithologies to those described by Partridge (1978). They proposed that basal sediment packages across boreholes 5, 1 and 4 (and maybe 3) represent Member 2. These boreholes do not transect the Silberberg Grotto (Pickering and Kramers, 2010; Herries and Shaw, 2011; Herries et al., 2013) and so have not been directly associated with the type section in the chamber. A flowstone at the base of the allogenic sequence in borehole 1 (sample BH1-15) yielded dates of 2.80 ± 0.28 Ma. Pickering and Kramers (2010) proposed that a thick flowstone defines the upper limit of Member 2 and base of Member 4, abandoning Member 3 as a distinct unit. Speleothem samples BH4-9 and BH1-8 were used to date the Member 2/Member 4 boundary and yielded ages of 2.650 ± 0.28 and 2.830 ± 0.344 respectively.

Here, we focus on those sediments that can be confidently stratigraphically associated with the type sediments of Member 2 as originally described by Partridge (1978) and so use the paleomagnetic ages of flowstones proposed by Herries and Shaw (2011) and Herries et al. (2013)—1.95 Ma at the top of the sequence to 2.58 Ma at the base—as the most suitable alternative ages to those proposed by Granger et al. (2015). The implications for the option 'B' calibration are that Member 2, along with StW 573, is contemporaneous with Member 4 (Pickering and Kramers, 2010; Herries et al., 2013) and accumulated between about 2 and 2.6 Ma, with the Silberberg Grotto filling from a vertical shaft at the same time as Member 4 accumulated, as originally proposed by Partridge (1978).

Here we must note that stratigraphic work focusing on the StW 573 specimen has demonstrated that four flowstones in the immediate vicinity of StW 573 (F1–F4 in Bruxelles et al., 2014), including flowstones 2B, 2C and 2D (Walker et al., 2006), are intrusive. These intrusive speleothems are not given stratigraphic unit labels. A further comprehensive study of each flowstone and its association with the clastic units beyond the immediate area of StW 573 is underway. This study focuses on the clastic sediments only as they more clearly reveal the nature of initial sediment deposition and postdepositional disturbance.

Recent application of a refined cosmogenic nuclide dating method yielded a date of 3.67 ± 0.16 Ma for the deposition of the sediments and clasts stratigraphically associated with the specimen (Granger et al., 2015). The association of one of these samples with the skeleton was recently questioned by Kramers and Dirks (2017a, b) who proposed a two-stage burial scenario for the sediments associated with the skeleton. For this to happen "it requires (1) an upper cave level environment in which the sediment accumulated over time, and (2) events in which the accumulated sediment matter, including chert fragments derived from within the cave, dropped to a deeper level in the form of debris flows and was chaotically mingled. Because the fossil was incorporated as an articulated skeleton, it cannot be older than the deposit, and the individual must, therefore, have fallen into the lower cave on its own, or incorporated in a debris flow." (Kramers and Dirks, 2017a: 51).

The result of these debates has been the emergence of two stances, a younger age of between 2.58 and 2.0 Ma and an older age 3.67 ± 0.16 Ma (Granger et al., 2015). The recent proposal of Kramers and Dirks (2017a, b) provided an additional formation hypothesis specifically for those sediments close to the StW 573 specimen and must also be considered.

Here we use sedimentological and stratigraphic evidence at multiple scales to clarify the formation processes of Member 2 and relate those processes to the depositional association and taphonomic history of the StW 573 skeleton. The stratigraphic control will help relate the formation processes to the greater system evolution and help test the physical manifestations of the above dating hypotheses (e.g., evidence of localized collapse, landscape stability, and sediment provenience).

1.3. Member 2 taphonomy

Pickering et al. (2004) identified the presence of antimeric and articulating specimens and the absence of carnivore modification, juvenile (dependent age) carnivore specimens, coprolites, and digested bone as evidence of an assemblage primarily accumulated through 'death-trap' processes. Extinct genera of primates (*Parapapio*), carnivorans (*Chasmaporthetes*) and bovids (*Makapania*) are present in an assemblage overwhelmingly dominated by primates and felids (Pickering et al., 2004). Pickering et al. (2004) suggested that animals with 'climbing proclivities' entered the Silberberg Grotto on their own, either by falling in or by accessing an entrance high in the ceiling of the Silberberg Grotto and subsequently being unable to escape. There is no evidence of a substantial role of carnivores in the accumulation process as demonstrated by the very

low percentages of such modifications—less than 6% of the primate assemblage and less than 3% of the non-primate assemblage (Pickering et al., 2004). The presence of a nearly complete and articulated *Australopithecus* skeleton with no observable biogenic modification (Pickering et al., 2004) supports the argument for a mainly death-trap accumulation process. In contrast with Member 4, StW 573 is the only hominin represented in the current Member 2 assemblage. Together, the skeleton from the western talus and the articulating remains of fauna from Dump 20 and from in situ blasting of the eastern talus demonstrate a consistent faunal accumulation mode across the Member 2 deposit (Pickering et al., 2004; Clarke, 2006).

1.4. Member 2 paleoenvironments

The cercopithecoid fauna of Member 2 is dominated by small-bodied papionins, such as *Parapapio jonesi*, *Parapapio broomi* and *Papio izodi*, along with one colobine species, *Cercopithecoides williamsi* (Pickering et al., 2004; Heaton, 2006). The Sterkfontein papionins were much smaller than modern-day species and exhibited lesser degrees of sexual dimorphism (Heaton, 2006, 2007). In contrast, fossil colobines were significantly larger (Delson et al., 2000) and have been used to argue for a clear terrestrial component in assemblages from eastern Africa (Jablonski et al., 2008). While *Cercopithecoides* from southern Africa are smaller, conclusions about their terrestrial proclivities have been extended to sites within the Sterkfontein valley (Ciochon, 1993; Elton, 2001). However, data from the papionins appear mixed. The postcranial anatomy of *P. jonesi* has been argued to indicate open areas, while the slightly larger *P. broomi* may have been arboreal (Elton, 2001). Maier (1970) suggested that *C. williamsi* would have lived near densely forested areas, possibly a tropical fringe forest along rivers of the nearby valleys. Similarly, Elton et al. (2016) argued that the primate species of Sterkfontein Member 2 were probably to some extent ecologically dependent upon trees for foraging or predator avoidance, or both. Among the papionins, a shift to larger body size, and perhaps greater territoriality, is not strongly indicated until Member 5 of the Sterkfontein Formation when there was a drier climate (Luyt and Lee-Thorp, 2003; Heaton, 2006, 2007).

The Member 2 mammalian fauna includes caracals, *Makapania*, and monkeys, and indicates a paleohabitat of rocky hills covered in brush and scrub and valley bottoms with riverine forest, swamp and standing water (Pickering et al., 2004). The base of the valley certainly retained year-round standing water because, even today, there is a perennial (if small) river in the valley bottom, and extensive remnants of river gravels below Sterkfontein and Swartkrans indicate that the river was larger and closer to the site in the past (Martini et al., 2003).

2. Methods

In order to answer the question of how Member 2 formed, several methodological approaches were applied across different scales. At the macroscale, the chamber geomorphology and major deposit geometry were incorporated (e.g., Tankard and Schweitzer, 1976; Goldberg and Bar-Yosef, 1998; Farrand, 2001; Osborne, 2001; Sasowsky and Mylroie, 2004; Stratford et al., 2012). At the mesoscale, sediment facies descriptions and fabric observations in specific sections were correlated laterally and longitudinally through the Silberberg Grotto to associate specific features within the larger depositional framework (e.g., StW 573, solution cavities, colluvial, alluvial and collapse facies). At the microscale, thin section samples target key sections (see Fig. 1 for sample locations) and are described to provide sedimentological support for formation processes identified at the mesoscale. Sections chosen for meso- and microscale assessment (Fig. 1) are associated with different areas of the Member 2 talus, which we consider to include all sediments that can be stratigraphically correlated with the StW 573 specimen, both upslope and downslope.

2.1. Cave mapping

The existing plans (Martini et al., 2003) were unsuitable for the required sections, so a speleological topographic map was drawn of the main axes of the cave, which were then associated to the surface excavation site. The profiles derived from these data are presented in the Discussion (Subsection 4.4).

2.2. Stratigraphy of the breccia

The processes of accumulation of Member 2 must be approached with a great caution. Depending on the origin of the sediments and their mode of accumulation, temporal and environmental associations with the fossils they contain can be misinterpreted. It is, therefore, important to know if Member 2 primarily accumulated through a gradual gravitational accretion of mostly surface-derived clastic material supplemented with sporadically collapsing blocks from the entrance or roof (Bruxelles et al., 2014; Stratford et al., 2017), or through a sudden introduction by a collapse or debris flows, for example with the collapse of an overlying gallery (Kramers and Dirks, 2017a, b).

The specific stratigraphic context of StW 573 (Bruxelles et al., 2014) was studied prior to its dating by Granger et al. (2015). The objective of the previous study was to illustrate the diachronic relationships between the flowstone units associated with StW 573 and the Member 2 clastic deposits. Here this work is expanded to document the clastic units laterally and longitudinally through the Member 2 sequence.

To understand the representative Member 2 sedimentation processes, four detailed stratigraphic sections were documented along the Silberberg Grotto Member 2 talus, as recognized by Partridge (1978), Martini et al. (2003), and Clarke (2006) –see Fig. 1. The sections incorporate the eastern end of Member 2 and the proximal part of the talus on both flanks of its apex. Two further sections were documented in the central part of the western slope of the talus (proximal-medial). For these sections, we describe each unit, its composition, organization, general fabric and stratigraphic association to the other recognized units, with particular attention paid to the organization of clasts and matrix (for mesoscale variables presented, see Table 1). A fifth, transverse section correlates the deposits inside the Silberberg Grotto with those in the Milner Hall.

2.3. Micromorphology

At the microscale, seven thin sections are presented that were strategically sampled through the exposed profiles of Member 2 in the Silberberg Grotto (Fig. 1) to better reveal the sedimentary structures that indicate the primary depositional processes (described as facies) of that unit. Three thin sections focus on facies within the proximal part of the eastern flank of Member 2. PE.A samples facies SA-5, PE.B samples SA-3, and PE.C samples SA-4 (Figs. 2 and 3). One thin section, PW.A, focuses on a thick unit within the proximal west flank of Member 2, SB-5. Two thin sections focus on two facies identified to be stratigraphically associated with the StW 573 specimen—M.A samples SC-4 (B2b in Bruxelles et al., 2014), and M.B samples the underlying SC-3 (B2a in Bruxelles et al., 2014). One thin section, M.C, samples unit SD-3 of the SD profile and was taken slightly downslope of the SD profile

Table 1
Summary of structural and sedimentological characteristics of the identified stratigraphic units within each documented section. See Figure 1 for location of documented sections.

Section	Unit	Sub unit	Thickness (cm)	Nature	General description	Support	Matrix color	Matrix texture	Clast size range	Clast abundance	Grading	Fabric	Bedded	Fossil abundance
A	SA-7		10	speleothemic	laminated flowstone	calcite	beige	–	–	–	–	–	yes	–
	SA-6		20	clastic and speleothemic	coarse to fine sandy breccia	matrix	light brown/pink	coarse to fine	small to medium	low	upwards fining	planar	yes	low
	SA-5		40	clastic	coarse sandy breccia	matrix	brown	coarse to loam	small to medium	low	no	planar	no	medium
	SA-4		150-30	clastic	bedded coarse sandy breccia	matrix	gray to brown	coarse	small	high to low	upwards fining	planar	yes	locally high
	SA-3		20	clastic	bedded stony with bone beds	matrix	reddish brown	sandy silt	small to medium	medium	graded subunits	linear and planar	yes	locally high
		SA-3b	10	clastic	stony to sandy mixed breccia	matrix	reddish brown to gray	sandy silt	small to medium	high to medium	upwards coarsening	planar to isotropic	yes	locally high
		SA-3a	10	clastic	bone bed sandy breccia	matrix	reddish brown	sandy silt	small	very low	no	linear and planar	yes	locally high
	SA-2		20–30	speleothemic	stony flowstone	calcite	white	–	medium	high	upwards coarsening	–	yes	–
	SA-1		>100	clastic	Member 1	matrix	black to gray	sandy	small to large	high	no	isotropic	no	–
B	SB-6		0–40	clastic	bedded reddish brown breccia	matrix	reddish brown to gray	silty sand	small to medium	medium to low	upwards coarsening	planar	yes	medium
	SB-5		60	clastic	stony breccia	matrix	reddish brown to gray	silty sand	medium	medium	graded subunits	planar	yes	high to medium
	SB-4		30–40	clastic	bedded reddish brown breccia	matrix	reddish brown	coarse to loamy sand	small to medium	medium	graded subunits	planar	yes	medium
	SB-3		50–70	clastic	bedded reddish brown breccia	matrix	reddish brown	coarse to loamy sand	medium	medium - stratified	no	planar	yes	low
	SB-2		>100	clastic	dark gray breccia	matrix	dark gray	sandy silt	small	medium	upwards fining	isotropic	yes	none
	SB-1		unknown	speleothemic	stony flowstone	calcite	white	–	medium	medium	no	–	yes	–
C	SC-6		20	speleothemic	F5 flowstone	calcite	white	–	–	–	–	–	yes	–
	SC-5		?	clastic	B3 gravely sand breccia	matrix	reddish	clayey sand	medium to large	medium	upwards fining	planar	yes	low
	SC-4		150	clastic	B2b stony breccia	clast	orange	clayey sand	medium	high	upwards fining	isotropic	no	high and StW 573
	SC-3		10–20	clastic	B2a	matrix	reddish brown	clayey sand	small to medium	medium	no	no	yes	low
	SC-2		30–40	clastic	B1 stony breccia	matrix	reddish brown	clayey sand	small to medium	medium	no	planar	yes	low
	SC-1		unknown	clastic	pink stony breccia	matrix	pink	sandy	medium to large	high	–	planar	–	low
D	SD-4		10–20	speleothemic	flowstone	calcite	white	–	–	–	–	–	–	–
	SD-3		30–40	clastic	stony breccia	matrix	reddish brown	clayey sand	medium	high	graded subunits	planar	yes	low
	SD-2		40–50	clastic	orange bedded breccia	matrix	orange	sandy silt	medium	medium	no	planar	yes	low
	SD-1		unknown	clastic	pink stony breccia	matrix	pink	sandy	medium to large	high	no	planar	yes	low

for logistical reasons. The samples were embedded with polyester resin, cut, mounted and polished to 30 μm thickness at the Thin Section Laboratory, School of Geosciences, University of the Witwatersrand (Johannesburg, South Africa). They were then studied by R.M. and D.J.S. in plane-polarized and cross-polarized light. Microphotography was conducted at the Microscopy and Microanalysis Unit (MMU) at the University of the Witwatersrand using an Olympus BX63 petrographic microscope, automated sliding stage and Olympus DP 80 camera. Photographs were taken with a 4× objective under plane-polarized light (PPL) cross-polarized light (XPL). The primary objective of this approach was to provide microscale sedimentological support to the mesoscale observations and provide additional detail on the origin of the sediments. Detailed micromorphology and geochemical analyses are ongoing and will be presented elsewhere.

3. Results

3.1. Member 2 stratigraphy

The four detailed sections studied (Fig. 1b) allow the stratigraphy of Member 2 to be followed along the length of the chamber, incorporating StW 573 and highlighting the lateral and longitudinal facies variation along the slope. Facies characteristics from each section are summarized in Table 1 and described through their respective sequences below.

Section A—Silberberg Grotto, eastern end This section (Fig. 2; Supplementary Online Material [SOM] Fig. S1) summarizes the observations made in the eastern end of the Silberberg Grotto where mining and blasting have exposed the complete depth of the unit across the width of the chamber. From the bottom up, we note the following succession:

SA-1: The base of the wooden staircase rests on a dark breccia comprised of blocks of chert and dolomite of all sizes within a sandy black-gray matrix cemented by calcite. This breccia corresponds to Member 1 (Partridge, 1978; Martini et al., 2003).

SA-2: A calcite flowstone several decimeters thick conforms to the irregularities of the Member 1 breccia surface and embeds abundant blocks of chert. The abundance of blocks increases towards the top and becomes a chert breccia cemented by a calcite matrix. The top of this flowstone is relatively irregular and forms a dome in the central part of the section, descending along the irregular flanks of Member 1. This represents the boss speleothem formed on the autogenic, clastic Member 1.

SA-3: A reddish brown stony breccia overlies the flowstone. This level is not continuous in the section because it conforms closely to the topography of the underlying flowstone. The gradient is shallow, only a few degrees dipping towards the east. At the eastern end, the unit divides into two. At the base, formed conformably on the SA-2 flowstone, a layer of about 10 cm consists mostly of bones embedded in an east sloping stratified, poorly indurated sandy-silty matrix with very low clast abundance. The abundant long bone fossils have been sorted but also, through deposition, are oriented in the direction of the slope (E–W).

Conformably overlaying this unit is about 10 cm of matrix-supported clasts and bones, which are organized in a planar fabric, although in some areas bones show linear fabric. This unit grades into a stony breccia with fragments of chert, dolomite, calcite concretions and bones.

SA-4: The stony breccia is covered by a thick formation of microbreccia with infrequent dolomite and chert clasts. In detail, this formation is comprised of decimeter-thick layers that can be followed along the length of the exposure. The granulometric sorting of these microbreccia emphasizes the stratification of this formation and indicates some hydrodynamic sorting. Several darker layers that are very rich in microfaunal remains are also present (Fig. 3). In the upper levels, discrete lenses of clasts and several thin strata of gravel can be seen.

SA-5: Conformably overlying SA-4, coarse sandy facies continue. At about 40 cm thick, the unit has a very low frequency of chert and dolomite clasts. Here the bedding is less visible but those bones that can be seen have a planar fabric conforming to the dip of the bedded layers, representing a succession of layers sloping eastwards.

SA-6: Coarse sands grade into lighter and clearly laminated fine sands containing fossil bones. Small layers of calcite are interbedded between some fine sand layers, indicative of an entrance in the process of closing.

SA-7: The section is sealed by a finely laminated beige calcite flowstone. Continuous all along the exposure, this speleothem is visible throughout the upper eastern part of the Silberberg Grotto, where the above unit (Member 3) was deposited conformably onto it. Such conformable deposition contrasts with the cavity-filling speleothem where formation of vertically downward forming speleothem fills a void (Bruxelles et al., 2014). This speleothem indicates a significant break in the clastic filling of the chamber and was identified by Partridge (1978, 2000) and Partridge and Watt (1991) as unit 3A. This speleothem provides a stratigraphic distinction between Member 2 breccia and the overlying Member 3.

Section B—Silberberg Grotto, west talus (proximal) Fifteen meters down the western flank and topographically lower than Section A (Fig. 1b), the proximal section of the western slope of Member 2 has been exposed in a deep mining trench cut to access the thick speleothem covering Member 1. From the bottom up, we have noted the following succession (Fig. 4; SOM Fig. S2):

SB-1: A partial concave casting of the thick Member 1-covering speleothem (the 'boss') is still preserved in the base of this unit's breccia, which conforms to the steeply west dipping Member 1, not exposed anywhere west of this section.

SB-2: To the east and at the base of the section, this breccia conformably rests against the boss. Where the breccia has formed directly onto Member 1, the contact is abrupt and erosional. Bedding is present and it is delineated by strata of chert clasts which are more abundant at the base. Dark gray in color, this unit represents the reworking of the altered dolomite and residual chert clasts of Member 1. SB-2 formed along a slope created by the initial conical accumulation and subsequent erosion of Member 1.

SB-3: After an erosive unconformity, a coarse breccia with a reddish brown matrix-supported deposit formed. This 50–70 cm thick unit formed locally on the boss speleothem, whose imprint is still visible. The unit consists of an alternating sequence of coarse sands and small clasts within massive sandy loam layers. Within subunits, clasts retain a planar fabric. Some bones are visible in the exposure and are arranged according to the angle of repose of the slope.

SB-4: Lying conformably above is a less indurated 30–40 cm thick relatively clast-poor unit supported by a sandy matrix. Bedding is noticeable in the upper part with discrete clast-rich lenses with consistent angles of repose. Differential induration of breccia within the unit also demonstrates the bedding.

SB-5: The uppermost unit exposed in the section consists of about 60 cm of matrix-supported stony breccia that formed conformably onto SB-4. Discrete stony subunits interstratify the silty-sand matrix. The base of this formation is clearly distinguished by a relative abundance of bones with strong fabric development according to the slope and orientation of the

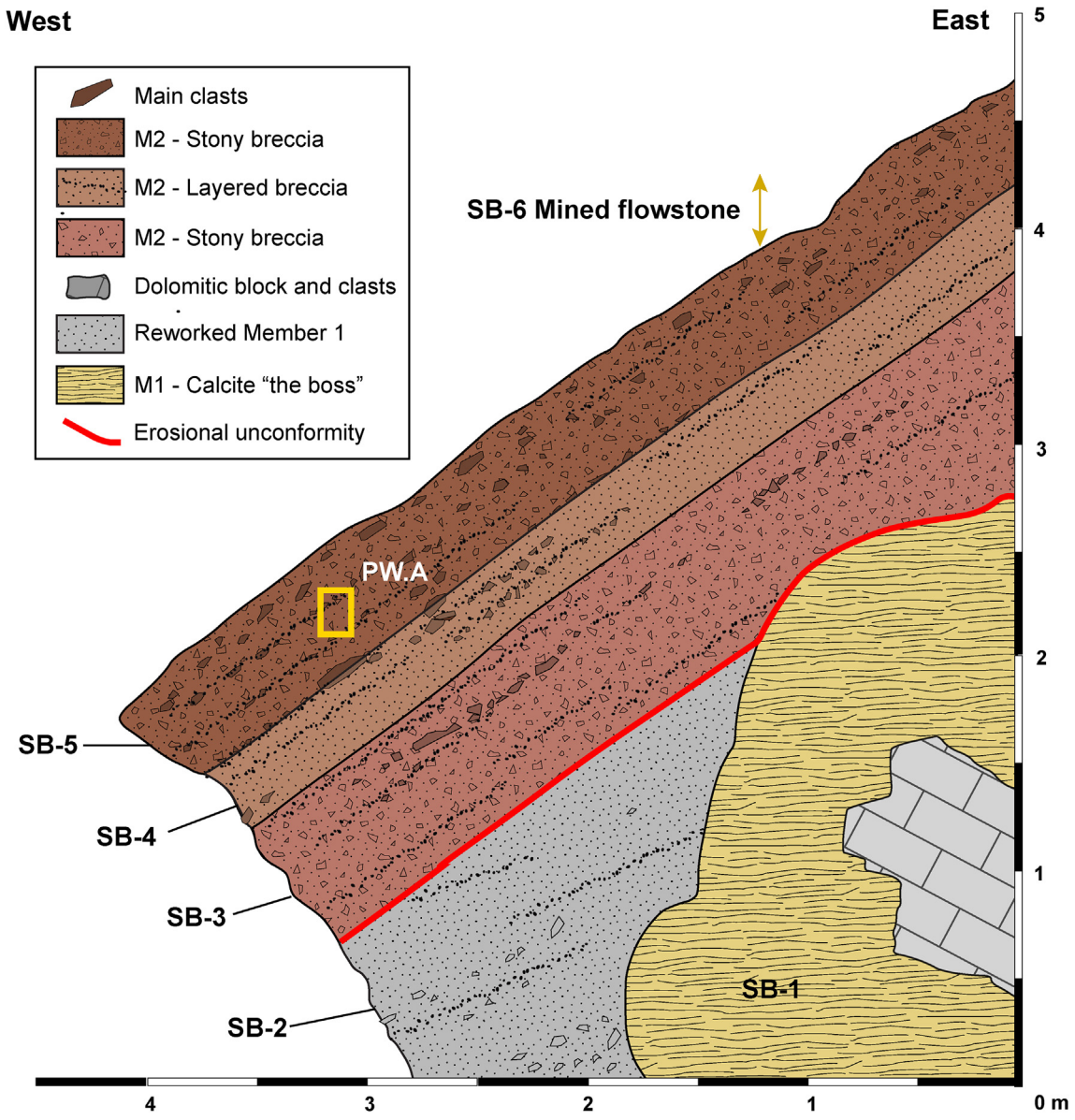

Figure 4. Synthetic representation of Section B (see Fig. 1b for location).

deposits. Remnants of SB-4 and SB-5 are preserved on the southern wall, opposite the Section B exposure, and display the same sedimentological and fabric characteristics demonstrating the previous continuation of these units across the N-S width of the Silberberg Grotto.

SB-6: The upper sedimentary reaches of the exposed section were mostly destroyed during mining. Between the current surface of SB-5 and the roof there could have been other layers of breccia. But these would not be very thick because a calcite flowstone which previously sealed this part of the deposit can be seen laterally, adhering to the roof only 20–30 cm above the surface of SB-5. From the remnant exposures, SB-6 is generally a fine reddish breccia of irregular thickness.

Section C—Silberberg Grotto, west talus (medial) The section of the western talus published by Bruxelles et al. (2014) focused on understanding the relationship between speleothem units and the StW 573-bearing breccia. Section C here focuses on the distinction of the different facies present in Member 2 in this area of the deposit, and it documents a new vertical exposure close to where StW 573 was discovered. Section C is advantageously orientated along an E–W axis of the gallery, longitudinally through the slope of Member 2 (consistent with the geometry of the clastic deposits) and in an area where the stratigraphy is less disturbed by the presence of filling speleothem units. To aid comparisons across space, the deposits distinguished are labeled with additional reference to those described in Bruxelles et al. (2014): breccia (B) and calcite (F). From the bottom up, we observe the following succession (Fig. 5; SOM Fig. S3):

SC-1: At the current floor of the chamber, a stony breccia of pinkish color has been poorly exposed by mining activity and is difficult to describe in detail. It is a sandy matrix-supported breccia with poorly sorted clasts of a few centimeters to one decimeter in maximum dimension.

SC-2: The nature of the contact between SC-1 and the overlying finer, orange SC-2 unit is difficult to discern. Rich in fine clay/silt matrix, the unit contains some small scattered subrounded

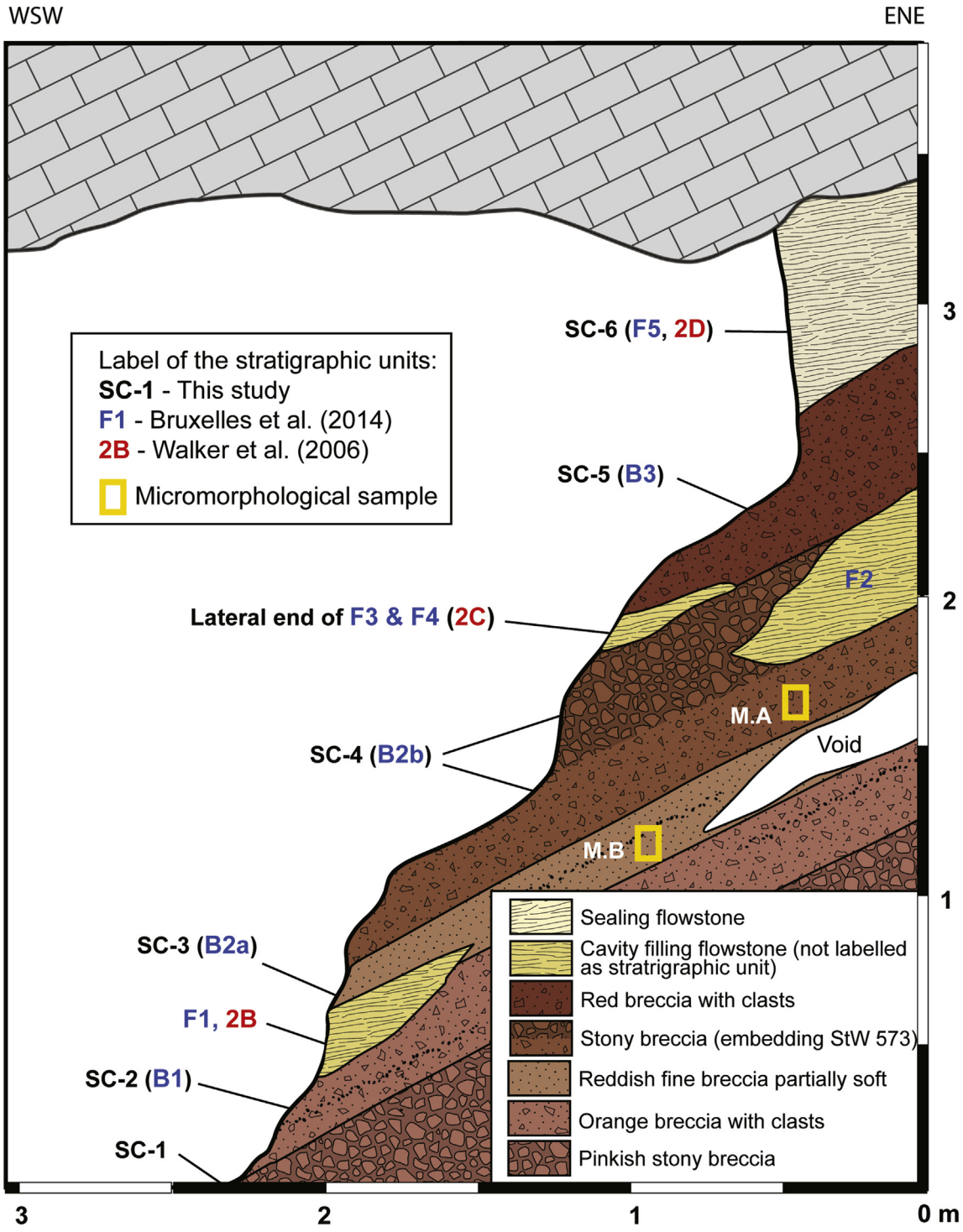

Figure 5. Synthetic representation of Section C (see Fig. 1b for location). Flowstones identified in Walker et al. (2006) and Bruxelles et al. (2014) are correlated. In this study dedicated to clastic deposits, intrusive flowstones are not labeled as distinct stratigraphic units.

clasts and angular blocks. This breccia corresponds to B1 in Bruxelles et al. (2014).

SC-3: Above, a relatively poorly cemented massive matrix-supported unit is present that is potentially secondarily altered. The poorly indurated nature of this unit has allowed the excavation of localized voids by water and the partial or complete secondary filling of those voids with calcite (B2a and F1; Bruxelles et al., 2014). The low, elongated shape of these voids, often sloping at thirty degrees towards the west, indicates the initial geometry of the unit. Clasts gradually become more abundant in the upper level of this unit and discernable decimetric blocks and smaller associated clasts conform to the same angle of repose of the voids and visible sedimentary contacts.

SC-4: SC-3 grades into a clast-supported unit (B2b in Bruxelles et al., 2014) associated with the StW 573 skeleton and several elements of non-hominin primates and carnivores in

fragmentary and complete condition. Poorly sorted and poorly organized medium to large (10 cm) blocks are abundant and cemented within a reddish sand matrix.

SC-5: The contact between SC-4 with SC-5 is locally disturbed by the presence of infiltrating calcite flowstones secondarily interstratifying the unit (F3 and F4 in Bruxelles et al., 2014). This brownish red silty-sand matrix-supported breccia with scattered small clasts and discernable bedding (B3 in Bruxelles et al., 2014) is of irregular thickness because it was partially destroyed by the mining of an overlying speleothem unit.

SC-6: This speleothem unit seals the breccia deposits in this part of the Silberberg Grotto (F5 in Bruxelles et al., 2014). Despite being targeted by miners, it is still visible in section along the west gallery, where it fills the residual voids between the low roof and the uppermost layers of breccia inclined to the west.

Section D—Silberberg Grotto, west talus (medial) A final section was documented in the western end of the Silberberg Grotto (Fig. 1b). The section allows us to observe the continuation of recognized breccia units beyond and downslope of StW 573, confirming their continuity and the consistency of the sedimentary processes that governed their formation. Only the lower part of the sequence observed in Section C is exposed here because of the presence of a dolomitic pendant, the upper sediments of which were either eroded away or were removed through mining (Fig. 6 a,d; SOM Fig. S4):

SD-1: At the base of the exposed sequence (the floor of the chamber is not visible), a stony matrix-supported breccia is present with abundant medium to large (10 cm) blocks of chert and dolomite within a pink sandy matrix. Clasts display some fabric organization and indicate a dominant east to west slope. This unit corresponds to SC-1 of Section C.

SD-2: An orange unit abruptly overlies SD-1 and is a finer, poorly consolidated matrix-supported deposit partially interstratified by infiltrating calcite speleothem. It corresponds to SC-2. As in SC-3, the shape and repose of the speleothem correspond to the shape of the voids they have filled, the latter being guided by the initial stratification of the unit and its differentially indurated internal bedding. Discrete lenses of small clasts are present and dip westwards, conforming to the overall geometry of the nearby units and stratigraphic contacts.

SD-3: This matrix-supported bedded unit conformably overlies SD-2. At its base is a bed of poorly sorted subrounded to angular clasts that spread from east to west with individual clasts

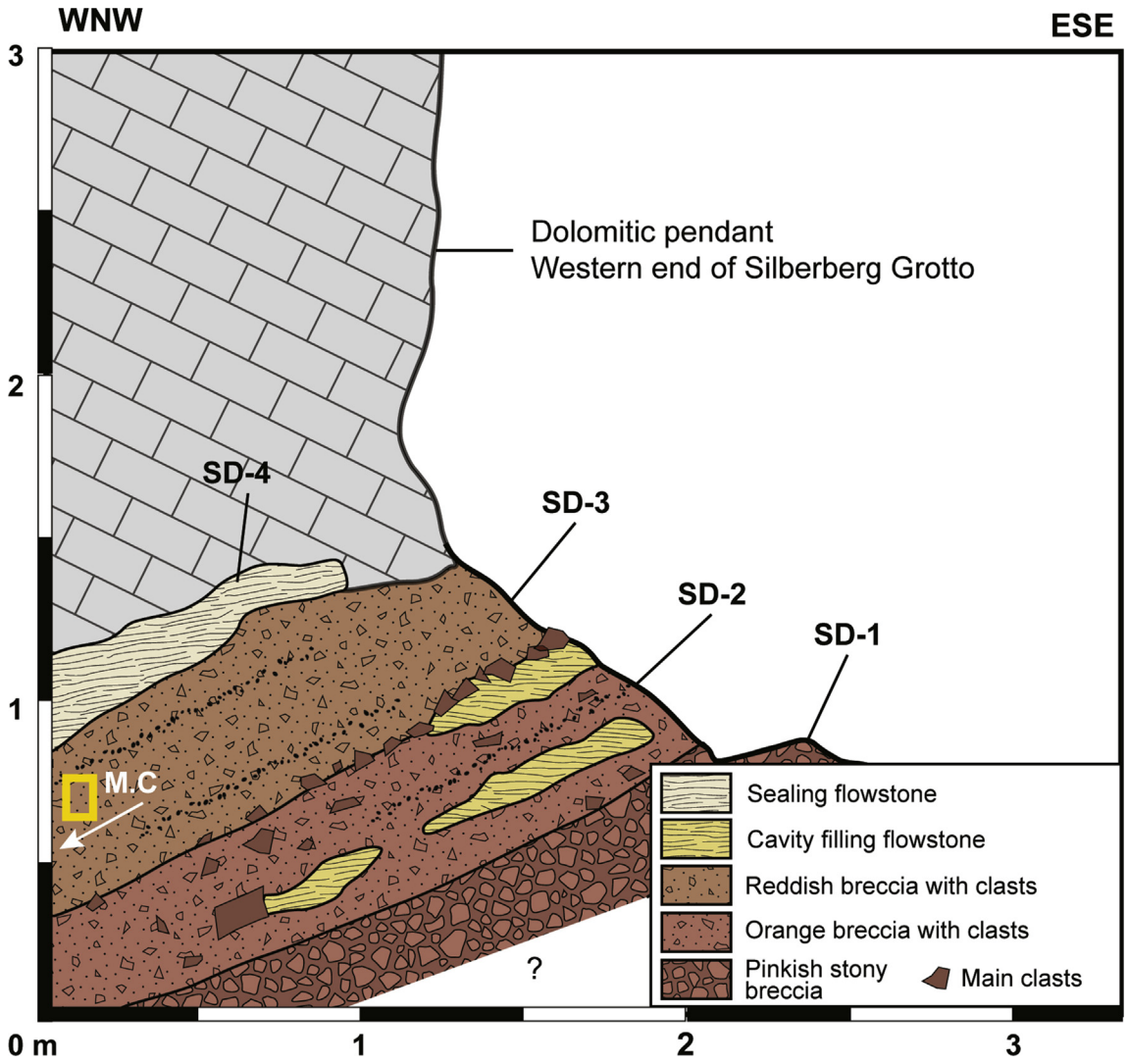

Figure 6. Synthetic representation of Section D (Western end of Silberberg Grotto, see Fig. 1b for location).

showing strong fabric development, indicating an angle of repose of about 30° east to west.

SD-4: This speleothemic unit fills the gap between the top of SD-3 and the bottom of a dolomitic pendant.

3.2. General thin section features

Although dedicated micromorphological analysis is ongoing, we describe here the major structures and features of the sediments and relate those to the prevailing formation processes involved in the development of the corresponding part of the talus and Member 2 in general. The location of each thin section sample in relation to the Silberberg Grotto and described sections can be seen in Figure 1. Below, the general features are described before each sample description is presented in Subsection 3.3 from east to west across the Member 2 talus.

Framework Generally, the framework in all samples is an aggregated composition of infrequent small to medium clasts within an orange/red/brown and dark matrix of iron- and manganese-rich sandy silts that show varying levels of pedogenic aggregation. In situ decay/reworking has modified dolomites, broken down soil aggregates, and distributed manganiferous and ferruginous silts.

Structure Structures are massive to stratified (e.g., PE.A, PE.C and PW.A) with occasional lamination and significant postdepositional calcite infiltration.

Clasts These are: variably abundant, poorly sorted, angular to rounded chert clasts; small, subrounded to rounded dolomite clasts; small, rounded lateritic clasts with quartz grain inclusions; and rounded sandy pedogenic aggregates representing fragments of lateritic crusts. Clasts often have decayed surfaces and ferruginous coatings.

Matrix The orange/red/dark brown matrix is generally massive and composed of coarse to fine mono- and polycrystalline quartz grains, and relatively abundant manganiferous and ferruginous lateritic silts deriving from pedogenic alterites represented as individual grains, aggregates, and particle and pore space coatings. Variability in density is often due to variable induration of calcite.

Voids Large void spaces are generally infrequent, elongated to rounded, dispersed and isotropic. Small voids are more abundant and form fine, irregular isotropic to linear networks occasionally associated with bedding planes, clasts and bioclasts. Voids are partially to completely filled with postdepositional calcites including aragonite and sparite.

Postdepositional modification Postdepositional void formation and filling with calcite has locally caused dispersion of sandy grains and iron (Fe) and manganese (Mn)-rich silts that fill voids and locally form coatings on clasts and individual particles. No distinct evidence is seen for the in situ breakage of clasts and fossil bones or fragmented speleothems or deformation through compression or collapse. Some postdepositional corrosion of chert and dolomite clasts is evident.

3.3. Individual thin sections

We present annotated figures of PE.B (Fig. 7) and PE.C (Fig. 8) in plane-polarized and cross-polarized light to illustrate the general features representative of the samples. Figures of the other thin section samples are presented in SOM Figures S5–S9.

PE.A This sample (SOM Fig. S5) is composed of: frequent poorly sorted angular, tabular and rounded chert clasts; subrounded to rounded dolomite clasts; rounded dark brown/black ferruginous and manganiferous clasts with quartz inclusions; and infrequent rounded sandy aggregates of pedogenic origin. Tabular and elongated particles tend to be horizontally or subhorizontally orientated, perhaps indicating remnant structure and stratification. Most clasts have a dark Fe and Mn coating. The infrequent uncoated clasts represent contributions by autogenic cave breakdown. Some dolomite and chert clasts show heavy pedogenic weathering.

The orange/red matrix is generally massive and composed of fine grains of quartz, with small to medium-sized fragments of bone and silt, and is further indurated by the postdepositional calcite. Abundant manganiferous and ferruginous lateritic coating of grains occurs. Void spaces are frequent and larger voids are

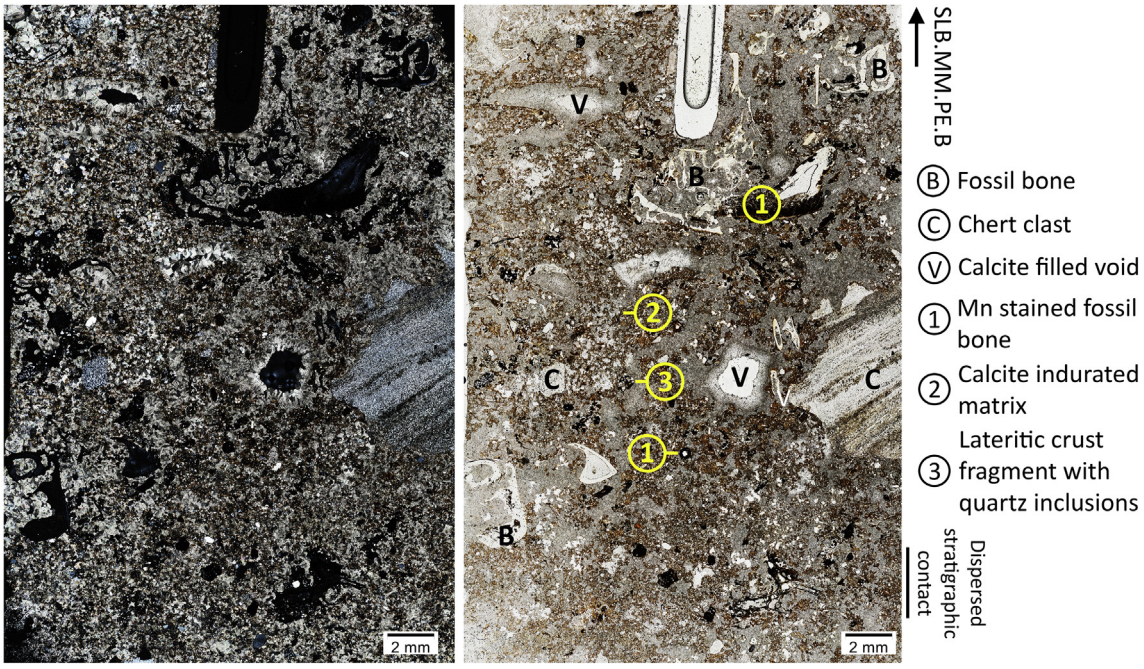

Figure 7. Sediment micromorphology sample PE.B (see Figs. 1b and 2 for location) with key features and inclusions indicated. Right microphotograph is plane-polarized light, left microphotograph is cross-polarized light. Arrow indicates orientation of sample and scale is shown on each image.

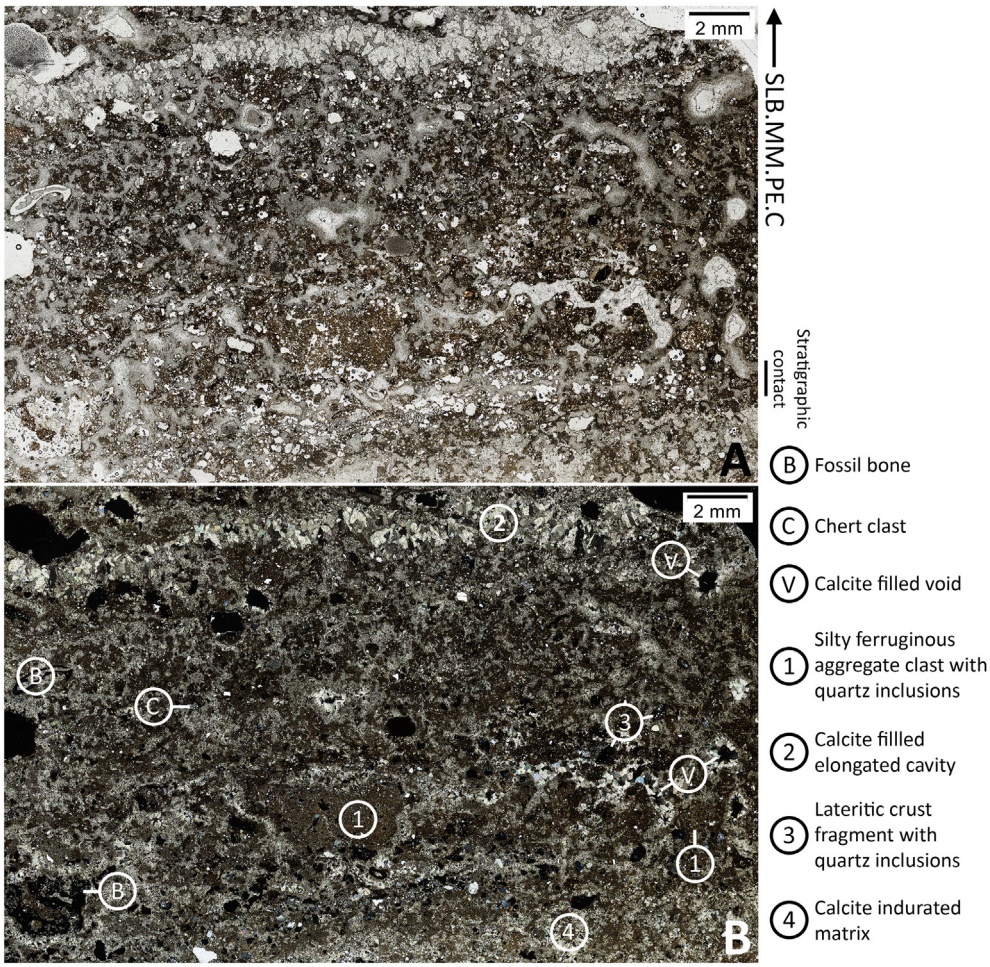

Figure 8. Sediment micromorphology sample PE.C (see Figs. 1b and 4 for location) with key features and inclusions indicated. Upper microphotograph is plane-polarized light, lower photograph is cross-polarized light. Arrow indicates orientation of sample and scale is shown on each image.

elongated and vertically orientated and partially or totally filled with calcite.

PE.B This sample (Fig. 7) is composed of abundant void-filling calcite within a massive matrix, infrequent clasts that have little to no Fe and Mn coating, and abundant poorly sorted angular cancellous and cortical fossil bones fragments. Chert clasts are generally poorly sorted, rounded to subrounded, with the notable presence of a large chert clast. Abundant rounded lateritic clasts (some with quartz inclusions) are present. Dolomite clasts are infrequent, rounded and decayed.

The orange/red matrix is generally massive and composed of fine grains of quartz and small to medium-sized fragments of bone within a clay and silt groundmass. Manganiferous and ferruginous silts fill voids and partially penetrate fossil bones fragments. Structure is unclear due to abundant postdepositional calcite.

Void spaces are abundant, variable in size and shape, and form irregular networks that pervade the sample and are frequently directly associated with clasts (including bioclasts) and decayed aggregated sediments. Voids are partially or totally filled with calcite.

PE.C This sample (Fig. 8) is a stratified sediment with few clasts. Small, subangular to subrounded clasts of dolomite (in various states of decay) and occasional large rounded bioclasts are distributed through the sample. Stratification is underlined by a large elongated void filled with sparitic calcite. Poorly sorted, rounded sediment aggregates are also present and more abundant in the lower half of the sample. Below this level, small, sorted angular sand-sized quartz grains are associated with generally horizontal strata and have been dispersed by postdepositional void formation and calcite filling.

The orange/red matrix is generally massive between stratum boundaries and composed of fine grains of quartz and small to medium-sized fragments of bone within a silty clay ferruginous groundmass. Manganiferous and ferruginous silts are more abundant in the upper half of the sample as lateritic grains, silty grain coatings, void fillings, or they adhere to poorly preserved sediment aggregates.

Voids are infrequent, occasionally rounded, but generally form irregular networks that spread horizontally across the sample conforming to the bedding of the sediment.

PW.A This sample (SOM Fig. S6) is composed of infrequent, poorly sorted subangular to subrounded chert clasts, small subrounded to rounded dolomite clasts and infrequent rounded lateritic aggregates of pedogenic origin with small quartz grain inclusions. Chert clasts are partially coated with manganiferous and ferruginous silts and coatings are generally restricted to the upper surface. Clasts are better sorted and more abundant in the upper reaches of the sample.

The orange/red/dark brown matrix is generally massive and composed of coarse to fine quartz grains. Relatively abundant manganiferous and ferruginous lateritic silts present as individual grains, aggregates and particle and pore space coatings and fillings.

Large void spaces are infrequent, round in shape and irregularly dispersed through the sample. Small voids are abundant and

characterized by fine irregular networks extending roughly horizontally across the sample. Voids are both unfilled and filled by calcite, and some show possible generational dissolution and deposition of different calcite forms.

M.A For this sample (SOM Fig. S7), the framework is an aggregated composition of clasts of poorly sorted angular (few) to smaller rounded chert clasts (2–5 mm) and ferruginous, rounded indurated red-orange grains (2–10 mm) of sandy sediments of pedogenic origin and irregular dark brown to black ferruginous and manganiferous lateritic grains with few quartz inclusions. Dolomite clasts are rare, small and rounded. Clasts show no organization and are not directly associated. Fe and Mn coated laterite fragments are also observed associated with angular to rounded poorly sorted mono- and polycrystalline quartz grains.

The orange/red ferruginous matrix is composed of fine grains of quartz and fragments of bone. Silty sand matrix is further indurated by the postdepositional calcite, with partially or totally filled voids. Void spaces are generally small and widely distributed, and larger voids are elongated and isotropic.

M.B This sample (SOM Fig. S8) is a generally massive sediment composed of fine sand and millimetric fragments of chert with ferruginous soil aggregates. Clasts are small, rare, poorly sorted, rounded to subrounded with Fe and Mn coatings. Infrequent small rounded dolomites are present in various stages of decay. Clasts show no organization and are not directly associated. Structurally, the sediments are less aggregated than in M.A. Some grains show very dark coatings of manganese and ferruginous grains of orange-red goethite type are present.

The orange/brown matrix is composed of fine quartz grains and ferruginous and manganiferous silts and clays penetrated by a cementation of white calcite. Large void spaces are generally infrequent, elongated to rounded, and restricted to the upper portion of the sample, dispersed and isotropic. Small voids are abundant and are not filled with calcite.

M.C In this sample (SOM Fig. S9), two layers are present: a dark, upper layer and a lighter lower layer. The upper layer is composed of poorly sorted angular to rounded chert clasts, the majority of which has Fe and Mn coatings (some more angular chert clasts have no coatings at all), occasional well-preserved bone fragments and infrequent grains composed of ferruginous lateritic silts and clays with rounded poorly sorted quartz inclusions. Clasts are more abundant in the upper part of the upper unit.

The upper brown-red unit matrix is generally massive, heavily indurated and composed of fine quartz and iron and manganese-rich groundmass with no clear aggregates present. Voids are abundant, and calcite fills larger elongated and perpendicular void networks with a strong left to right inclination. Small voids pervade the sample and almost all voids are filled with calcite in the upper unit.

The lower unit is clast-poor and heavily indurated and shows a ‘chopsticks’ of manganese crusts. Clasts are sorted, rounded to subrounded, and made up of chert and quartz. Some remnant soil aggregates may be present. The unit is dominated by white sparitic calcite with a low density of clay-ferruginous matrix. Many small, unfilled voids are visible throughout the matrix with a possible role of a secondary dissolution phase.

4. Discussion

4.1. Global geometry of Member 2 deposit from macro- and mesoscale data

The geometry of Member 2 in the Silberberg Grotto indicates the deposit formed a single talus cone, the apex of which is located towards the eastern end of the chamber (Fig. 1b) beneath an original entrance which fed the chamber and is now choked. On the eastern flank, the east-dipping Member 2 is sealed by a calcite flowstone (SA-7 here; Unit 3A in Partridge, 1978) separating it from the overlying breccia (Member 3 in Partridge, 1978). The western flank of the Member 2 talus is clearly observable due to its exposure by extensive speleothem mining in the central and western areas of the chamber. The western flank slopes at a 30–40° angle of repose westwards towards the Elephant Chamber for almost 30 m before exiting the Silberberg Grotto through three passages.

The general shape of the talus is partly influenced by the basal Member 1 breccia and its covering boss speleothem, which here we consider to be part of the autogenic Member 1 formation process. During the vadose collapse of the cave, a process that formed Member 1, the thickest Member 1 deposits formed where there was greatest decay of the dolomite, i.e., where faults in the dolomite are most abundant on the southern boundary of the system (Stratford, 2017). The highest part of the roof of Silberberg Grotto is in the east, the area where the largest amount of dolomite and chert material was removed to the base of the chamber during the vadose, joint-governed collapse, forming a talus of chert blocks encased in a black-gray sandy matrix that was subsequently cemented by calcite (i.e., Member 1 and the associated boss speleothem). The collapse of the roof in the eastern area of the chamber also thinned the overlying host rock (relatively), enabling increased vertical water movement, precipitation of speleothem, and ultimately the potential for the development of an entrance above the Member 1 talus. All erosive and depositional processes found in the Silberberg Grotto originate from this location. The eroded western flank of Member 1 dips more steeply than the eastern flank, a morphology that has partially controlled the distribution and resulting asymmetrical geometry of Member 2, with sediments preferentially being deposited to the west (Sections B, C and D). The eastern flank (Section A), shallower in angle of repose, received less sediment than the western flank but with a greater influence of fluvial processes as observed by Partridge (1978) and Clarke (2006) and evidenced by the sorted and well-orientated fossil bones exposed in the eastern breccia wall.

As observed by previous researchers (e.g., Partridge, 1978; Martini et al., 2003), the Member 2 talus geometry indicates that the deposit's entrance is located vertically to the apex. At the macroscale, surveys from the Silberberg Grotto to the landscape surface (Fig. 9a) revealed that there is no dolomite above the highest point of the talus and the remnants of a vertical conduit are present, still filled with breccia. Immediately above this point, on the surface, is the southern-most extent of a solution cavity-riddled breccia of Member 4 (Fig. 1a). We therefore do not observe a contact between Member 3 and Member 4 in this area. It may be that Member 3 is very thin here, the contact is near vertical (as is often the case close to walls and entrances), or the contact has been mixed; alternatively, there is no contact in this area. The nature of the upper contact of Member 3 is therefore crucial to our understanding of the middle units of the Sterkfontein Formation.

From inside the Silberberg Grotto, Member 3 ascends nearly vertically to the ceiling, its morphology governed by the shape of the boss speleothem around which it formed. The lower contact of Member 3 is clearly distinguished from Member 2 by an intercalating flowstone (SA-7 in Fig. 2; Unit 3A in Partridge, 1978 and Partridge and Watt, 1991; sample S3 in Partridge et al., 1999). On the western talus a speleothem unit sealed Member 2. Much of this was mined away in the proximal sections of the talus as it formed close to, and in places onto, the boss speleothem, but we recognize it as correlating with SA-7, SC-6 and SD-4. In section B, remnants of this may adhere to the ceiling above the mined unit (with remnants preserved) SB-6. This speleothem has been sampled for paleomagnetic dating (S3 in Herries and Shaw, 2011) and yielded a

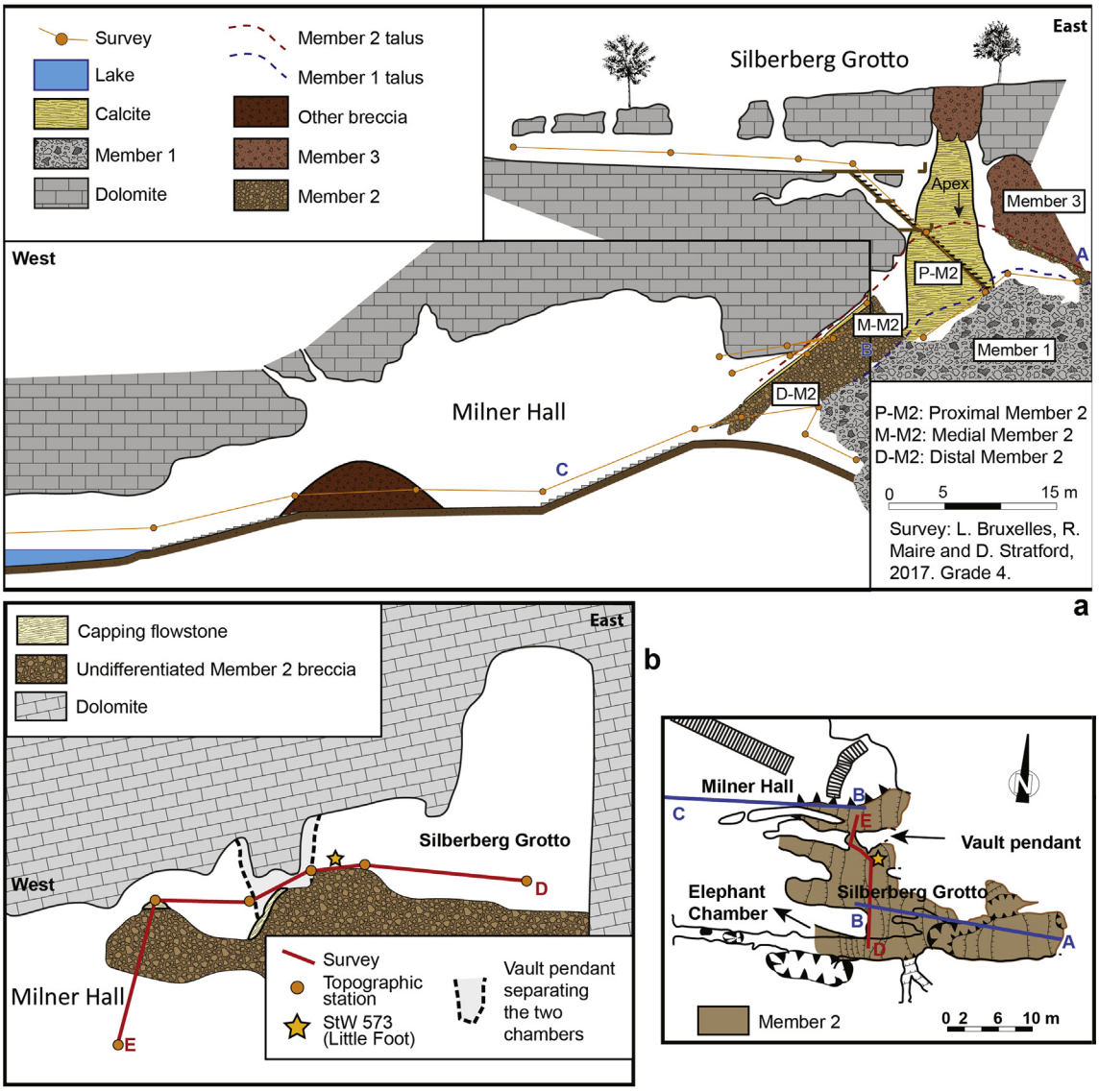

Figure 9. a) Global section along the Member 2 talus, from Silberberg Grotto to the Milner Hall (see Fig. 1b for location). b) Transverse N-S section through the Member 2 Talus from the Milner Hall to the Silberberg Grotto through a small passage. This survey demonstrates the continuity of Member 2 sediments between the two chambers which are separated by a remnant E–W orientated dolomite pendant.

normal magnetic polarity originally calibrated to the 2.58 Ma Matuyama/Gauss boundary or 1.78–1.95 Ma (Partridge et al., 1999; also see 'Option A and B' in Herries et al., 2013). If the cosmogenic dates of Granger et al. (2015) are correct then this speleothem formed under normal global magnetic polarity and may relate to the Gauss-Gilbert boundary, dated to 3.60 Ma (Ogg, 2012).

The general shape of the talus, the inclination of the slope (between 30 and 40°), and the longitudinal profile of the slope, which is slightly concave towards the base, are indicative of a colluvial talus (Kirkby and Statham, 1975; Statham, 1976; Postma, 1986; Brochu, 1978; Perez, 1989; Sæter, 1998; Bertran and Texier, 1999; Bertran et al., 1995, 1997). The proximal part, located at the apex, a medial part which is visible all along the western part of the Silberberg Grotto, and a distal part can be observed. The distal part, more difficult to observe because of mining damage, can be tracked into the Elephant Chamber and Milner Hall (Stratford et al., 2014). The macro- and mesoscale mapping demonstrates that the slope of Member 2 is continuous and coherent from apex to the Elephant Chamber and the Milner Hall. The implication is that the whole depth of the system was formed prior to significant opening to the surface, and early Member 2 sediments accumulated toward the base of the system (as suggested by Wilkinson, 1973, 1983; Stratford et al., 2014). This challenges the karstification model suggested by Partridge (1978), Partridge and Watt (1991), and Pickering and Kramers (2010).

In the eastern part of the Milner Hall, a stony breccia remains cemented against the south wall with a preserved surface inclined at 38° westward (SOM Fig. S10). This heavily undercut deposit can be followed for about 20 m, from the eastern end of Milner Hall East up a continuous slope through a narrow passage articulating with the Silberberg Grotto about 10 m below StW 573 (Fig. 9b). This indicates that the breccia in the Milner Hall has the same origin (as shown by the transverse section, F9b) and the same geometry (Fig. 9a) as Member 2 in Silberberg Grotto and represents a lateral and longitudinal continuity of Member 2 (Stratford et al., 2014).

4.2. Member 2 breccia accumulation

The mesoscale and microscale evidence collected through Member 2 makes it possible to identify varying modes of talus accretion. This is a crucial step to understanding the taphonomy of the faunal assemblage, as well as the association between sedimentary features and interred fossils, particularly StW 573, whose association with the nearby flowstones and sediments has been the subject of debate concerning the dating of the specimen (e.g., Clarke, 2002b; Pickering and Kramers, 2010; Granger et al., 2015; Kramers and Dirks, 2017a,b; Stratford et al., 2017).

First, it is clear that Member 2 is stratified through its entire thickness along the length of the talus (sections A to D; Fig. 1). Whether east or west of the entrance, several successive breccia units can be distinguished and linked to the structures and features found in the thin sections. All samples show variable abundances of the same composition of primarily allogenic materials with varying degrees of modification and infrequent inclusion of autogenic clasts. All thin sections indicate the gradual erosion of well-developed lateritic soils on the surface (as suggested by Stratford et al., 2014 from sediments attributed to an early distal portion of Member 2), contributing an iron-rich sandy matrix composed of a variety of soil aggregates, well weathered chert clasts, fossil bones fragments, and a notably infrequent contribution of coated dolomite clasts (dolomitic clasts being relatively quickly weathered away in soils on the landscape surface). Internally-derived clasts of dolomite and chert are uncoated, fresh and angular and do not represent the dominant clast contribution in any sample.

In Section A, the earliest infilling of breccias are documented, covering the Member 1 breccia and the boss speleothem. The stony and bone-rich breccia (SA-3) molds the irregularities of the Member 1 dome. It constitutes the very first level of allogenic breccia coming from the outside and is the result of the opening of an entrance above the apex of the talus, where the vault was the highest. This level of stony breccia (SA-3) could correspond to SB-3 in the proximal medium talus and the unit partly mined out at the base of Section C (SC-1 and SD-1; Fig. 10)—with finer composition generally associated with more proximal facies of the same unit.

Above, still in section A, the unit SA-4 is coarse breccia of variable thickness. This breccia is also stratified and shows a progressive accumulation by fluid run-off, which alternates between detrital layers, deriving from the erosion of the surface soil, and beds rich in microfauna. SA-4 can be correlated to SB-4 and SC-3 (and perhaps SC-2) further downslope to SD-2 (Fig. 10), which demonstrates an increase in clast size and abundance due to longitudinal sorting typical of colluvial deposits. A tentative correlation can also be made between SA-5, SB-5 and SC-5, suggesting the development of SC-4 as a discrete, stratified unit. Or perhaps the correlation is between SB-5 and SC-4 and SC-5, suggesting a thickening of SB-5 downslope. Across these sections we find the same facies successions, all in geometric coherence with the layers that can be connected following a slope of 30–40°.

Along the slope, the particle size of the clasts and the proportion of matrix vary from the proximal portion to the distal portion of the slope. This is entirely consistent with formation processes found in a colluvially accumulated talus (Statham, 1976; Kirkby and Statham, 1975; Brochu, 1978; Perez, 1989; Sæter, 1998; Bertran and Texier, 1999; Bertran et al., 1995, 1997; Sæter, 1998, 1998; Bruxelles et al., 2017). Proximal facies are characterized by finer sediments and generally lower abundance and smaller sizes of clasts. The distal facies of the slope are characterized by large blocks, most often without fine matrix, and the voids between the clasts can be subsequently filled by reworked sediments and calcite. In the medial part of the talus, facies distributions are variable and discrete stony layers can be locally preserved—like SC-4, the unit in which StW 573 was found. The longitudinal stratigraphic correlations along slope and the associated variability in clast abundance and size indicate that Member 2 was deposited primarily through gradual colluvial processes with sediments sourced locally from a slowly eroding landscape (Granger et al., 2015) covered in potentially well-developed lateritic soils (Moeyersons and De Ploey, 1976; Osborne, 1978, 2001; Mihevc et al., 1998; Pederson et al., 2000; Martini et al., 2003; Kos, 2001; Martini, 2011; Klimchouk, 2006; White, 2007;

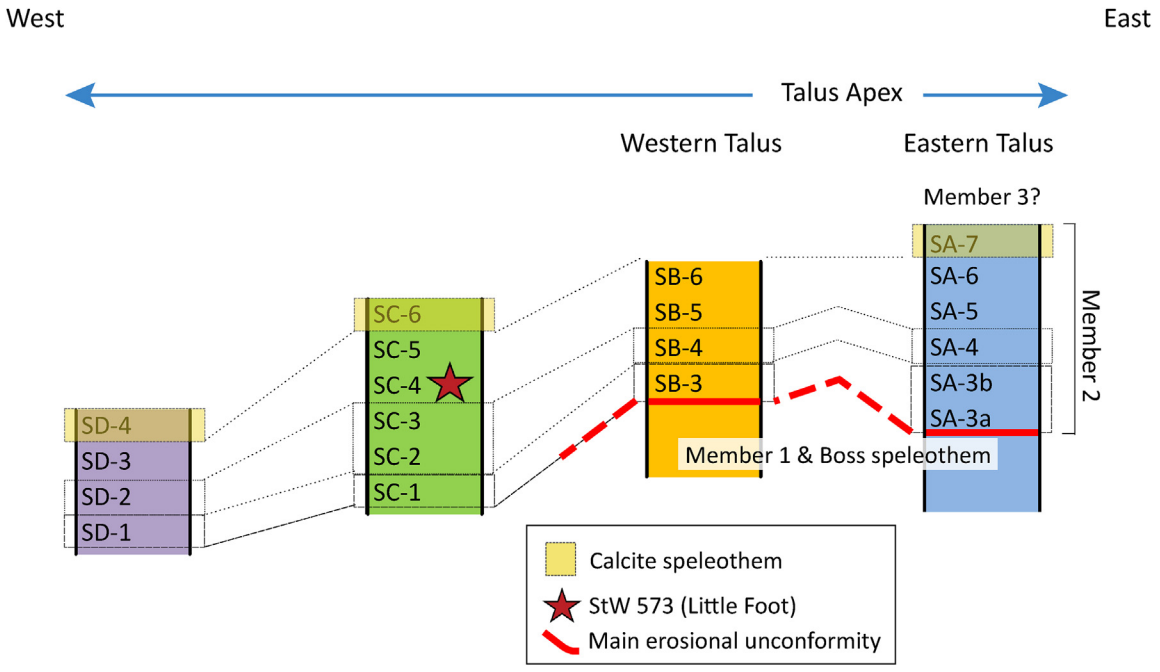

Figure 10. Proposition of correlations of the different sedimentary layers through the Member 2 talus in the Silberberg Grotto.

Bruxelles et al., 2017). Sediments accumulated through the high aven-like entrance above the eastern end of the chamber. Deposits were added to sporadically by relatively slow breakdown of the walls and the vault, as evidenced by infrequent, uncoated and angular dolomite clasts.

4.3. Taphonomy of StW 573

A detailed account of the taphonomy of the StW 573 specimen is provided by Clarke (2019) and follows previous observations presented in Clarke (2002b). In addition, we here discuss the position of the StW 573 body in relation to the sedimentary history of Member 2. Importantly, StW 573's body is orientated parallel to and at the angle of repose of the underlying and overlying deposits. It can be proposed that body fell onto the apex of the slope, directly beneath the opening in the eastern end of the chamber, and rolled perpendicular to the slope for 10 m down the western flank. Rotation of the body to a perpendicular orientation stabilized the body on the slope and the specimen's leg passed over the right as it came to a stable position with the left arm upslope above the body. Postdepositional modifications are all local events with no evidence of mass movements of stone or matrix observable in the specimen's preservation or associated sedimentary units above, below or laterally. Localized breakage can be limited to single events (although not necessarily at the same time) of isolated impact, compaction or subsidence, with broken bones, culprit clasts and voids, and associated fragments all remaining associated until excavation. The body position, mummification (Clarke, 2002b) and localized vertical disruption of skull and central part of the body (into the cavity below, as opposed to downslope movement) all indicate a solitary deposition of the specimen, a gradual burial and spatially isolated postdepositional modification, all correlating with the general sedimentary history of Member 2.

4.4. Member 2 breccia formation hypotheses

New multiscale research presented above provides the sedimentological and geomorphological evidence to scrutinize previous Member 2 breccia formation hypotheses more closely. Below, the hypotheses are discussed in relation to the evidence presented above.

An age of 2.58–2.2 Ma for StW 573 and Member 2 in the Silberberg Grotto has been proposed (Herries and Shaw, 2011; Herries et al., 2013). The dating of flowstones in the cave network below the Silberberg Grotto yielded relatively young ages (<400 to > 100 ka; Pickering and Kramers, 2010), supporting the epiphreatic karstification formation model proposed by Partridge (1978) and Partridge and Watt (1991). In this model, Member 2 represents the basal allogenic sedimentary deposit at Sterkfontein, with a series of deeper passages and chambers forming later and being filled by younger or reworked sediments. Macroscale mapping of Member 2 has provided crucial clues to test this hypothesis. This work instead confirms suggestions by Wilkinson (1973, 1983) and Stratford et al. (2014) that Member 2 previously extended beyond the Silberberg Grotto into the deeper caverns of the Elephant Chamber and the Milner Hall. Distal remnants matching the geometry of Member 2 can be found adhering to the roof and walls of the eastern Milner Hall and can be traced close to the current base level (Stratford et al., 2014). The sediments represented there are characteristic of distal facies of colluvially accumulated deposits with 30–40° gradients, consistently demonstrated in the bedding of Member 2 both inside and outside the Silberberg Grotto. This evidence increases the vertical and longitudinal distribution of Member 2.

Micromorphological evidence suggests the slow accumulation of well-developed lateritic soil aggregates and relatively low energy postdepositional modification of those soil structures. Structurally, the facies are similar to colluvial cones associated with slowly accreting 'overland flows' (Bertran and Texier, 1999), although subaerial modifications (e.g., rain splash) are limited in this context and postdepositional modification and void development differ due to the calcite intrusion. A limited catchment area of sediments around a relatively small opening near the top of the Sterkfontein hill also suggests a relatively limited source of sediments and low sedimentation rate. Mesoscale documentation of facies through the Silberberg Grotto allows us to correlate the sedimentary units longitudinally. Association of the identified facies variation longitudinally and vertically through the deposits allows the unification of the entirety of Member 2 into a single sedimentary and geometric spatially constrained framework. It is clear that colluvial processes dominate facies development and variability, forming coarser facies at the distal end and finer facies at the proximal end (Fig. 10).

In response to Granger et al. (2015), Kramers and Dirks (2017a, b) suggested that the stratigraphic and chronological association between StW 573 and Member 2 may be more complex. They posited that StW 573 and the sediments associated with it were subjected to a 'two-stage burial scenario', with StW 573 collapsing from a chamber above that is now eroded away. The mixing of sediments and the StW 573 specimen would constitute the formation of a 'secondary' deposit and therefore should be evident in the structure and composition of the deposits around StW 573. While we recognize that the original entrance to the Silberberg Grotto may now be where M4 south is, the entrance having been choked by Member 3, the location of the collapse proposed by Kramers and Dirks (2017a) is beyond the known eastern extent of the Silberberg Grotto and is east of the Member 2 talus apex (Stratford et al., 2017). Localized collapse above the western end of the chamber would be the only process that would enable the secondary deposition of a completely articulated skeleton. Directly above the skeleton is in situ roof. In addition, collapse deposits in caves are generally characterized by increased abundance of angular autogenic clasts, isotropic fabrics and fragmented speleothems and fossil bones. A specific reply was given by Stratford et al. (2017) regarding the macroscale and taphonomic implications of such a scenario, but further investigation was needed to clarify the association of the sediments close to StW 573 with the broader depositional framework to test their hypothesis, which we have done here.

Structurally, no evidence was found suggesting localized collapse in the vicinity of the specimen. SC-4 (B2b in Bruxelles et al., 2014) conforms to the geometry and organization of the bounding units and can (although tentatively at this point) be correlated to the more proximal unit SB-5. Voids, clasts and bioclasts below, within and above conform to a consistent 30–40° east to west slope suggesting regular bedding of all the Member 2 units, including SC-4. In thin section, samples M.A and M.B show no compositional difference to the other samples in terms of abundance of autogenic clasts and no distinct structures indicative of collapse microfacies. The generally low abundance of angular autogenic particles suggests slow internal chamber and entrance breakdown. The absence of fragmented speleothem, a common indicator of collapsed chambers, is absent at the meso- and microscales. The sediments have developed through the same processes as the other sampled units throughout the deposit. Taphonomically, although StW 573 is the only articulated full skeleton in Member 2, articulated and antimeric elements are found in the abundant fauna closely associated with the specimen, and as discussed above, postdepositional modification of the specimen is limited to localized and isolated low energy events affecting individual parts of the articulated skeleton, with each modification being preserved in its primary

modifying context (i.e., bones, clasts, voids, and fragments are still associated). The articulation of the left lower arm and hand is an excellent example of this, with clasts still associated at the breakage points of the radius and ulna and slightly displaced wrist bones. This would not be expected in a collapse scenario with turbulent movement of clasts, bones and sediments. It would also not be expected if the mode of initial burial or subsequent movement were through debris flow mechanisms, where a mass movement of clasts and sediments create turbulent flows and clast-supported lateral and longitudinal lobes (e.g., Van Steijn and Coutard, 1989; Bertran and Texier, 1994; Iverson, 1997; Coussot and Meunier, 1996; Major, 1998; Jameson, 1999; Bertran and Coussot, 2004; Jakob, 2005). Sedimentary structures indicative of debris flow processes are not evident in any of the Silberberg Grotto Member 2 exposures.

5. Conclusions

The multiscale evidence presented above has sought to test recent hypotheses regarding the stratigraphic and chronological history of Member 2 and the StW 573 specimen. Utilizing these tools provided the opportunity to clarify not only the history of the infilling of the Silberberg Grotto, but also the source and processes of accumulation of the Member 2 sediments and their association with the StW 573 skeleton. We do not provide new dates for the specimen but attempt to find supporting stratigraphic and sedimentological evidence to test the hypotheses put forward by Pickering and Kramers (2010) that some of the sediments in the western Silberberg Grotto may not be Member 2 and that the deposit is restricted to the Silberberg Grotto, in support of proposals by Partridge (1978) and Partridge and Watt (1991) for an epiphreatic karstification process forming the caves.

Our work has also addressed the recent proposal by Kramers and Dirks (2017a,b) that a single sample included in the 11 sample cosmogenic nuclide isochron published by Granger et al. (2015) could indicate reworking of sediments and a two-stage burial scenario for the StW 573 skeleton involving a collapse from an upper chamber. We have drawn upon the most recent stratigraphic work conducted by Bruxelles et al. (2014), Stratford et al. (2014) and absolute dates for Member 2 and the StW 573 specimen proposed by Granger et al. (2015) to reconstruct the sedimentary sequence. An explanation for the isolated cosmogenic sample dating to a younger age than the other samples could be the detachment of the fragment from the upper walls or roof which was afforded less shielding and so yields a younger isotopic age.

The sequence of deposits associated with 'Member 2' (as originally identified in the Silberberg Grotto by Partridge, 1978) can coherently be linked to the evolution of the Silberberg Grotto and includes the formation of the chamber, the opening of the entrance high in the roof, geometric constraints of the first allogenic infillings, episodic sedimentary hiatuses, differential sedimentary processes conforming to the geometry of the chamber, and final infilling and precipitation of the sealing calcite speleothem which represents the end of the Member 2 sequence. Throughout the sequence a consistent sedimentary framework is identified, which typifies many of Sterkfontein's deposits, characterized by slow accretion through colluvial talus development. The consistent bedding, concave longitudinal shape of Member 2 and longitudinal facies development are all characteristic of this mode of accumulation and attest to a slow accumulation with no distinct major collapses. Stratigraphic and facies correlations can be made that unify the deposit from its eastern flank exposures through to the remnants adhering to the walls and roof of the Milner Hall, confirming its previously proposed extent close to the current base level (Wilkinson, 1973, 1983; Stratford et al., 2014). The extension of Member 2 into the Milner Hall thus challenges the limitation of depth of Member 2 and the epiphreatic karstification model proposed by Partridge (1978) and Partridge and Watt (1991), suggesting the complete depth of the caves as we see it now had been developed at the time of its opening to the surface and that the deepest chambers may contain the oldest deposits (e.g., Wilkinson, 1973, 1983).

Microscopically, the similarities between samples indicate the same general accumulation process and suggest a slowly eroding landscape with allogenic sediments contributed from well-developed lateritic soils and slow autogenic cave breakdown but extensive localized calcite modification. A distinct lack of coated dolomite clasts and low frequency of uncoated, angular dolomite or chert clasts support a gradual mode of accumulation with no obvious collapse facies found through the sequence. The relatively gentle stratigraphic history of Member 2 supports the taphonomic history of not only the StW 573 specimen, but also the abundant other faunal remains which remain articulated and free from extensive biogenic or postdepositional modification. In conclusion, the evidence presented here supports the long development of a previously very large Member 2 and challenges the formation hypotheses made by Pickering and Kramers (2010) and Kramers and Dirks (2017a), along with the associated implications for the alternative younger age for StW 573.

Acknowledgements

We hereby acknowledge the support of the AESOP + program, the Claude Leon Foundation, the DST-NRF Center of Excellence in Palaeosciences (CoE-Pal), The Palaeontological Scientific Trust (PAST), the French National Institute for Preventive Archaeology Research (Inrap), the Embassy of France in South Africa and the French Institute of South Africa (IFAS) towards this research. Major funding for the Sterkfontein excavations has been provided by National Research Foundation grants to K.K. (#82591 and 82611) and to D.S. (#98808) and by PAST, without whose support this research could not have been able to continue. We thank Andrea Leenen and Robert Blumenschine for their help in securing major corporate funding, including sustained support from Standard Bank and JP Morgan. Authors would also like to extend their gratitude to the anonymous reviewers and editors Sarah Elton and David Alba, whose comments significantly improved this manuscript. Opinions expressed and conclusions arrived at are those of the authors and are not necessarily to be attributed to the Center of Excellence in Palaeosciences.

Supplementary Online Material

Supplementary online material to this article can be found online at https://doi.org/10.1016/j.jhevol.2019.05.008.

References

Beaudet, A., Carlson, K.J., Clarke, R.J., de Beer, F., Dhaene, J., Heaton, J.L., Pickering, T.R., Stratford, D., 2018. Cranial vault thickness variation and inner structural organization in the StW 578 hominin cranium from Jacovec Cavern, South Africa. Journal of Human Evolution 121, 204–220.

Berger, L.R., Lacruz, R., de Ruiter, D.J., 2002. Brief communication: Revised age estimates of *Australopithecus*-bearing deposits at Sterkfontein, South Africa. American Journal of Physical Anthropology 119, 192–197.

Bertran, P., Texier, J.P., 1994. Structures sedimentaires dans un cône de flots de debris Vars, Alpes françaises méridionales. Permafrost and Periglacial Processes 5, 155–170.

Bertran, P., Francou, B., Texier, J.P., 1995. Stratified slope deposits: the stone-banked sheets and lobes model. In: Slaymaker, O. (Ed.), Steepland Geomorphology. Wiley, Chichester, pp. 147–169.

Bertran, P., Hetu, B., Texier, J.P., Van Steijn, H., 1997. Fabric of subaerial slope deposits. Sedimentology 44, 1–16.

Bertran, P., Texier, J.P., 1999. Facies and microfacies of slope deposits. Catena 35, 99–121.
Bertran, P., Coussot, P., 2004. Les coulees de debris. In: Bertran, P. (Ed.), Dépôts de pente continentaux: dynamique et faciès. Quaternaire suppl. 1, pp. 132–151.
Brochu, M., 1978. Disposition des fragments rocheux dans les dépôts de solifluxion, dans les éboulis de gravité et dans les dépôts fluviatiles : mesures dans l'Est de l'Arctique nord-américain et comparaison avec d'autres régions du globe. Biuletyn Peryglacjalny 27, 35–51.
Bruxelles, L., Clarke, R.J., Maire, R., Ortega, R., Stratford, D., 2014. Stratigraphic analysis of the Sterkfontein StW 573 *Australopithecus* skeleton and implications for its age. Journal of Human Evolution 70, 36–48.
Bruxelles, L., Maire, R., Couzens, R., Thackeray, J.F., Braga, J., 2017. A revised stratigraphy of Kromdraai. In: Braga, J., Thackeray, F. (Eds.), Kromdraai, A Birthplace of *Paranthropus* in the Cradle of Humankind. Sun Media, Bloemfontein, pp. 31–47.
Bruxelles, L., 2018. Des fantômes et des hommes. Le rôle de la fantomisation dans la formation des karsts à australopithèques d'Afrique du Sud. Karstologia 69, 1–8.
Ciochon, R.L., 1993. Evolution of the Cercopithecoid Forelimb—Phylogenetic and Functional Implications from Morphometric Analyses. University of California Press, California.
Clarke, R.J., Tobias, P.V., 1995. Sterkfontein member 2 foot bones of the oldest South African hominid. Science 269, 521–524.
Clarke, R.J., 1998. First ever discovery of a well-preserved skull and associated skeleton of *Australopithecus*. South African Journal of Science 94, 460–463.
Clarke, R.J., 2002a. On the unrealistic 'revised age estimates' for Sterkfontein. South African Journal of Science 98, 415–419.
Clarke, R.J., 2002b. Newly revealed information on the Sterkfontein Member 2 *Australopithecus* skeleton. South African Journal of Science 98, 523–526.
Clarke, R.J., Partridge, T.C., Granger, D.E., Caffe, M.W., 2003. Dating the Sterkfontein fossils. Nature 301, 596–597.
Clarke, R.J., 2006. A deeper understanding of the stratigraphy of Sterkfontein fossil hominid site. Transactions of the Royal Society of South Africa 6, 111–120.
Clarke, R.J., 2007. Taphonomy of Sterkfontein *Australopithecus* skeletons. In: Pickering, T.R., Schick, K.D., Toth, N.P. (Eds.), Breathing Life into Fossils: Taphonomic Studies in Honor of CK (Bob) Brain. Stone Age Institute Press, Bloomington, pp. 199–205.
Clarke, R.J., 2008. Latest information on Sterkfontein's *Australopithecus* skeleton and a new look at *Australopithecus*. South African Journal of Science 104, 443–449.
Clarke, R.J., 2013. *Australopithecus* from Sterkfontein Caves, South Africa. In: Reed, K., Fleagle, J., Leakey, R.E.F. (Eds.), Paleobiology of *Australopithecus*. Springer, New York, pp. 105–123.
Clarke, R.J., 2019. Excavation, reconstruction and taphonomy of the StW 573 *Australopithecus prometheus* skeleton from Sterkfontein Caves, South Africa. Journal of Human Evolution 127, 41–53.
Coussot, P., Meunier, M., 1996. Recognition, classification and mechanical description of debris flows. Earth-Science Reviews 40, 209–227.
Delson, E., Terranova, C.J., Jungers, W.L., Sargis, E.J., Jablonski, N.G., 2000. Body mass in Cercopithecidae (Primates, Mammalia): estimation and scaling in extinct and extant taxa. Anthropological papers of the American Museum of Natural History 83, 1–159.
Elton, S., 2001. Locomotor and habitat classifications of cercopithecoid postcranial material from Sterkfontein Member 4, Bolt's Farm and Swartkrans Members 1 and 2, South Africa. Paleontologica Africana 37, 115–126.
Elton, S., Jansson, A.U., Meloro, C., Louys, J., Plummer, T., Bishop, L.C., 2016. Exploring morphological generality in the Old World monkey postcranium using an ecomorphological framework. Journal of Anatomy 228, 534–560.
Farrand, W.R., 2001. Sediments and stratigraphy in rockshelters caves: a personal perspective on practice and pragmatics. Geoarchaeology: An International Journal 16, 537–557.
Goldberg, P., Bar-Yosef, O., 1998. Site formation processes in Kebara and Hayonim Caves and their significance in Levantine prehistoric caves. In: Akazawa, T., Aoki, K., Bar-Yosef, O. (Eds.), Neandertals and Modern Humans in Western Asia. Plenum, New York, pp. 107–125.
Granger, D.E., Gibbon, R.J., Kuman, K., Clarke, R.J., Bruxelles, L., Caffee, M.W., 2015. New cosmogenic burial ages for Sterkfontein Member 2 *Australopithecus* and Member 5 Oldowan. Nature 522, 85–88.
Heaton, J.L., 2006. Taxonomy of the Sterkfontein fossil Cercopithecinae: The Papionini of Members 2 and 4 (Gauteng, South Africa). Ph.D Dissertation, Indiana University.
Heaton, J.L., 2007. The Problematic Papionina of Sterkfontein Member 4, Gauteng, South Africa. American Journal of Physical Anthropology 132, 128-128.
Herries, A.I.R., Shaw, J., 2011. Palaeomagnetic analysis of the Sterkfontein palaeocave deposits: Implications for the age of the hominin fossils and stone tool industries. Journal of Human Evolution 60, 523–539.
Herries, A.I.R., Pickering, R., Adams, J.W., Curmoe, D., Warr, G., Latham, A.G., Shaw, J., 2013. In: Reed, K., Fleagle, J., Leakey, R.E.F. (Eds.), Paleobiology of *Australopithecus*. Springer, New York, pp. 21–40.
Iverson, R.M., 1997. The physics of debris flows. Reviews of Geophysics 35, 245–296.
Jablonski, N.G., Leakey, M.G., Ward, C.V., Antón, M., 2008. Systematic paleontology of the large colobines. In: Jablonski, N.G., Leakey, M.G. (Eds.), Koobi Fora Research Project Volume 6: The Fossil Monkeys. California Academy of Sciences, San Francisco, pp. 31–102.
Jakob, M., 2005. A size classification for debris flows. Engineering Geology 79, 151–161.
Jameson, R.A., 1999. Concept and classification of cave breakdown: An analysis of patterns of collapse in Friars Hole Cave System, West Virginia. In: Kastning, E.H., Kastning, K.M. (Eds.), Appalachian Karst. National Speleological Society, Huntsville, pp. 35–44.
Kirkby, M.J., Statham, I., 1975. Surface stone movement and scree formation. Journal of Geology 83, 349–362.
Klimchouk, A., 2006. Cave un-roofing as a large-scale geomorphic process. Speleogenesis and Evolution of Karst Aquifers 4(9), 1–11.
Kos, A.M., 2001. Stratigraphy, sedimentary development and paleoenvironnemental context of a natural accumulated pitfall cave deposit from south-eastern Australia. Journal of Earth Science 30, 769–779.
Kramers, J.D., Dirks, H.G.M., 2017a. The age of fossil StW573 ('Little foot'): An alternative interpretation of $^{26}Al/^{10}Be$ burial data. South African Journal of Science 113, 45–51.
Kramers, J.D., Dirks, H.G.M., 2017b. The age of fossil StW573 ('Little Foot'): Reply to comments by Stratford et al. (2017). South African Journal of Science 113, #a0222.
Luyt, C.J., Lee-Thorp, J.A., 2003. Carbon isotope ratios of Sterkfontein fossils indicate a marked shift to open environments c. 1.7 Myr ago. South African Journal of Science 99, 271–273.
Maier, W., 1970. New fossil Cercopithecoidea from the lower Pleistocene cave deposits of the Makapansgat Limeworks, South Africa. Paleontologia Africana 13, 69–107.
Major, J.J., 1998. Pebble orientation on large, experimental debris-flow deposits. Sedimentary Geology 117, 151–164.
Martini, J.E.J., 2011. Cave clastic sediments and implications for speleogenesis: new insights from the Mugnano Cave (Montagnola Senese, Northern Apennines, Italy). Geomorphology 134, 452–460.
Martini, J.E.J., Wipplinger, P.E., Moen, H.F.G., Keyser, A., 2003. Contribution to the speleology of Sterkfontein Cave, Gauteng Province, South Africa. International Journal of Speleology 32, 43–69.
McKee, J.K., 1996. Faunal Evidence and Sterkfontein Member 2 foot bones of early hominid. Science 271, 1301–1302.
Mihevc, A., Slabe, T., Šebela, S., 1998. Denuded caves — an inherited element in the karst morphology; the case from Kras. Acta Carsologica 27, 165–174.
Moeyersons, J., De Ploey, J., 1976. Quantitative data on splash erosion, simulated on unvegetated slopes. Zeitschrift fur Geomorphologie 25, 120–131.
Ogg, J.G., 2012. Geomagnetic polarity time scale. In: Gradstein, F.M., Ogg, J.G., Schmitz, M.D., Ogg, G.M. (Eds.), The Geologic Time Scale 2012, Vol. 1. Elsiever, Amsterdam, pp. 85–113.
Osborne, R.A.L., 1978. Structure, sediments and speleogenesis at Cliefden Caves, New South Wales. Helictite 16, 3–32.
Osborne, R.A.L., 2001. Petrography of lithified cave sediment. In: Rasteiro, M.A. (Ed.), Proceeding of the 13th International Congress of Speleology. Sociedade Brasileira de Espeleologigia, Brasilia, pp. 101–104.
Partridge, T.C., 1978. Re-appraisal of lithostratigraphy of Sterkfontein hominid site. Nature 275, 282–287.
Partridge, T.C., Watt, I.B., 1991. The stratigraphy of the Sterkfontein hominid deposit and its relationship to the underground cave system. Palaeontologia Africana 28, 35–40.
Partridge, T.C., Shaw, J., Heslop, D., Clarke, R.J., 1999. The new hominid skeleton from Sterkfontein, South Africa: age and preliminary assessment. Journal of Quaternary Science 14, 293–298.
Partridge, T.C., 2000. Hominid-bearing cave and tufa deposits. In: Partridge, T.C., Maud, R.R. (Eds.), The Cenozoic of Southern Africa. Oxford Monographs on Geology and Geophysics. Oxford University Press, Oxford, pp. 100–125.
Partridge, T.C., Latham, A.G., Heslop, D., 2000. Appendix of magnetostratigraphy of Makapansgat, Sterkfontein, Taung and Swartkrans. In: Partridge, T.C., Maud, R.R. (Eds.), The Cenozoic of Southern Africa. Oxford University Press, Oxford, pp. 126–130.
Partridge, T.C., Granger, D.E., Caffee, M.W., Clarke, R.J., 2003. Lower Pliocene hominid remains from Sterkfontein. Science 300, 607–612.
Partridge, T.C., 2005. Dating of the Sterkfontein hominids: progress and possibilities. Transactions of the Royal Society of South Africa 60, 107.
Pederson, J., Pazzaglia, F., Smith, G., 2000. Ancient hillslope deposits: missing links in the study of climate controls on sedimentation. Geology 28, 27–30.
Perez, F.L., 1989. Talus fabric and particle morphology on Lassen Peak, 71A. Geografiska Annaler, pp. 43–57.
Pickering, T.R., Clarke, R.J., Heaton, H.L., 2004. The context of StW 573, an early hominid skull and skeleton from Sterkfontein Member 2: taphonomy and paleoenvironment. Journal of Human Evolution 46, 279–297.
Pickering, R., Kramers, D., 2010. Re-appraisal of the stratigraphy and determination of new U-Pb dates for the Sterkfontein hominin site, South Africa. Journal of Human Evolution 59, 70–86.
Pickering, R., Kramers, J.D., Partridge, T., Kodolanyi, J., Pettke, T., 2010. Uranium/lead dating of calcite/aragonite layers in low-uranium speleothems from South Africa by MC-ICPMS. Quaternary Geochronology 5, 544–558.
Pickering, R., Kramers, J.D., Hancox, P.J., de Ruiter, D.J., Woodhead, J.D., 2011. Contemporary flowstone development links early hominin bearing cave deposits in South Africa. Earth and Planetary Science Letters 306, 23–32.
Postma, G., 1986. Classification for sediment gravity-flow deposits based on flow conditions during sedimentation. Geology 14, 291–294.
Sæter, M.T., 1998. Dynamics of talus formation by May-Britt. Master's Thesis, University of Oslo.

Sasowsky, I.D., Mylroie, J.W., 2004. Studies of Cave Sediments: Physical and Chemical Recorders of Climate Change. Kluwer Academic/Plenum Publishers, New York.
Statham, I., 1976. A scree slope rockfall model. Earth Surface Processes 1, 43–62.
Stratford, D., Bruxelles, L., Clarke, R.J., Kuman, K., 2012. New interpretations on the stratigraphy of the fossil and archaeology bearing deposits of the Name Chamber, Sterkfontein. South African Archaeological Bulletin 67, 159–167.
Stratford, D., Grab, S., Pickering, T.R., 2014. The stratigraphy and formation history of fossil- and artefact-bearing sediments in the Milner Hall, Sterkfontein Cave, South Africa: New interpretations and implications for palaeoanthropology and archaeology. Journal of African Earth Science 96, 155–167.
Stratford, D., 2017. A Review of the Geomorphological Context and Stratigraphy of the Sterkfontein Caves, South Africa. In: Klimchouk, A., Palmer, A., De Waele, J., Auler, A., Audra, P. (Eds.), Hypogene Karst Regions and Caves of the World. Springer International Publishing, pp. 879–891.
Stratford, D., Granger, D.L., Bruxelles, L., Clarke, R.J., Kuman, K., Gibbon, R.J., 2017. Comments on 'The age of fossil StW573 'Little Foot': An alternative interpretation of 26Al/10Be burial data'. South African Journal of Science 113. #a0213.
Tankard, A.F., Schweitzer, F.R., 1976. Textural analysis of cave sediments: Die Kelders, Cape Province, South Africa. In: Davidson, D.A., Shackley, M.L. (Eds.), Geoarchaeology, Earth Sciences and the Past. Westview Press, Boulder, pp. 289–316.
Tobias, P.V., Clarke, R.J., 1996. Reply to J.K. McKee, Faunal evidence and Sterkfontein Member 2 foot bones of early hominid. Science 271, 1301–1302.
Turner, A., 1997. Further remains of Carnivora (Mammalia) from the Sterkfontein hominid site. Palaeontologia Africana 34, 115–126.
Van Steijn, H., Coutard, J.P., 1989. Laboratory experiments with small debris flows: Physical properties related to sedimentary characteristics. Earth Surface Processes and Landforms 14, 587–596.
Walker, J., Cliff, R.A., Latham, A.G., 2006. U-Pb isotopic age of the StW 573 Hominid from Sterkfontein. South African Journal of Science 314, 1592–1594.
Wilkinson, M.J., 1973. Sterkfontein cave system: evolution of a karst form. Master's Thesis, University of the Witwatersrand.
Wilkinson, J., 1983. Geomorphic perspectives on the Sterkfontein australopithecine breccias. Journal of Archaeological Science 10, 515–529.
Wilkinson, J., 1985. Lower-lying and possibly older fossiliferous deposits at Sterkfontein. In: Tobias, P.Y. (Ed.), Hominid Evolution: Past, Present and Future. Alan R. Liss, New York, pp. 165–170.
White, W.B., 2007. Cave sediments and paleoclimate. Journal of Cave and Karst Studies 69(1), 76–93.